POLYAMIDE-IMIDE AND MONTMORILLONITE NANOCOMPOSITES

Ajit Ranade, M.Sc.

Thesis Prepared for the Degree of

MASTER OF SCIENCE

UNIVERSITY OF NORTH TEXAS

August 2001

APPROVED:

Nandika Anne D'Souza, Major Professor
Rick Reidy, Committee Member
Robert Wallace, Committee Member
Witold Brostow, Committee Member
Michael Kozak, Committee Member
Bruce Gnade, Minor Professor and Chair of the Department of Materials Science
C. Neal Tate, Dean of the Robert B. Toulouse School of Graduate Studies

Ranade, Ajit, Polyamide-imide and Montmorillonite Nanocomposites. Master of Science (Materials Science), August 2001, 95 pp., 2 tables, 57 illustrations, 67 references.

Solvent suspensions of a high performance polymer, Polyamide-imide (PAI) are widely used in magnetic wire coatings. Here we investigate the effect that the introduction of montmorillonite (MMT) has on PAI. MMT was introduced into an uncured PAI suspension; the sample was then cured by step-wise heat treatment. Polarized optical microscopy was used to choose the best suitable MMT for PAI matrix and to study the distribution of MMT in PAI matrix. Concentration dependent dispersion effect was studied by x-ray diffraction (XRD) and was confirmed by Transmission electron microscopy (TEM). Differential scanning Calorimetry (DSC) and Thermogravimetric analysis (TGA) was used to study impact of MMT on glass transition temperature (T_g) and degradation properties of PAI respectively. Micro-hardness testing of PAI nanocomposites was also performed. A concentration dependent state of dispersion was obtained. The glass transition (T_g), degradation and mechanical properties were found to correlate to the state of dispersion.

ACKNOWLEDGMENTS

My sincere thanks go to Dr. Nandika Anne D'Souza for her patience and encouragement. Under her guidance I learned how to conduct research and communicate my ideas.

Advice and suggestions from my thesis committee, Professor Rick Reidy, Professor Robert Wallace, Professor Witold Brostow, Professor Michael Kozak and Professor Bruce Gnade (minor advisor) are highly appreciated.

I would like to acknowledge Professor Teresa Golden for helping with x-ray diffraction studies. I would like to thank especially Dr. Kevin Menard for the discussion and help about thermal characterization. I would like to give sincere thanks to Professor William E. Acree for allowing me to use the optical microscope. I thank David Garrett for his help with TEM and SEM experiments. I also thank Dr. Jason Grigg for his help with micro-hardness testing. I gratefully acknowledge Doug Hunter, Southern Clay Products for recommendations on clay selections as well as materials. I also acknowledge J. Yodis and S. George of P.D. George company for the support of PAI.

This work would not have been possible without the continued input from friends and colleagues. I am grateful to the members of the Mechanical Testing and Rheology laboratory, both past and present. I especially like to thank Alejandro Hernandez-Luna for his continues help.

Finally I like to thank my parents, my sister and brother in law Makarand for never ending support, love and constant encouragement.

TABLE OF CONTENTS

Page

LIST OF TABLES

Page

LIST OF ILLUSTATIONS

Page

Chapter 1

INTRODUCTION

When two or more phases are mixed together to make a composite, a combination of properties that are not available in any of the individual components is possible. Nanocomposites offer useful new properties compared to conventional materials with relatively small amounts (2-5%) of nanometer sized clay particles[1-54]. All of these benefits are obtained without significantly raising the density of the compound or reducing light transmission (nanoclays are in the same size range as visible light wavelengths). The word “nanocomposite” refers to composites whose reinforcement has at least one dimension in the nanometer scale. The nano scale filler is a pristine mica type layered silicate. The advantage of these nano scale ceramic fillers (clays) is their nanoscale morphology (1nm thick & 100-1000nm in length). Because the building blocks of a nanocomposite are nanoscale, they have enormous surface area leading to high interfacial area between filler and matrix. The special properties of the nanocomposite arise from the interactions of its phases at the interfaces[1-26]. By contrast, in a conventional composite based on micron sized fillers such as carbon fibers and glass fibers, the interfaces between the filler and matrix constitute a much smaller volume fraction of the bulk material and therefore influence its properties to a much smaller extent.

Nanocomposites find applications in various fields such as automobile industry (exterior and interior body parts), packaging industry (bottles, containers, plastic films

and fuel tanks), electronic industry (packaging materials and exterior parts of electronic devices). Coating industry (paints, wire enamel coatings etc) and aerospace industry (body parts of airplane and exterior surface coatings)[55,56,57].

To make a successful nanocomposite, it is very important to be able to disperse the inorganic material throughout the polymer and create those interfaces. If a uniform dispersion is not achieved, clumps of inorganic material end up inside the polymer, which does not lead to desirable properties[1-20]. It is also important, to split the silicate "deck of cards" into individual cards because dispersing those cards allows more polymer to be affected with less filler.

Factors limiting successful dispersion of the layered silicates are the hydrophilic nature of the silicates and largely hydrophobic nature of most engineering polymers. To produce the intercalated nanocomposite, the polymer has to wet the clay particles to some extent so that the polymer chains are intercalated between the clay galleries. To make delaminated or exfoliated nanocomposites, a higher degree of wetting is required[1,2,11-16,22,25,52].

To counter the problem of particle agglomeration, the clay interlayer surfaces of the silicate are chemically treated to make the silicate less hydrophilic and therefore more wettable by the polymer. This is accomplished by cation exchange process where hydrophilic cations such as Na^+ K^+ and Ca^{2+} are exchanged by alkyl ammonium cations. The role of alkyl ammonium cations in the organosilicates is to lower the surface energy of the inorganic host and improve the wetting characteristics with the polymer. The

length of the alkyl ammonium cations determines the hydrophobicity of silicate layers[2,11-16,31,52].

Nanocomposites have many advantages over conventional composites such as[1-26]

- *Improved mechanical properties:* The dispersed platelets dramatically increase the polymer's stiffness and strength without sacrificing its toughness.
- *Improved scratch resistance*: This is critical in automobile paints and nanocomposite coatings.
- *Optical properties*: Montmorillonite nanocomposites absorb ultraviolet light (UV). This property would help to protect the polymer, which is degraded by UV light.
- *Improved heat distortion temperature (HDT)*: Increased dimensional stability at elevated temperatures due to the rigid reinforcements increases the HDT. Nanocomposites also reduce shrinkage and warpage of the host polymer.
- *Barrier properties:* Nanocomposites can slow transmission of gases and moisture vapor through plastics by creating a "tortuous path" for gas molecules to thread their way among the obstructing platelets resulting in reduced permeability to gases, moisture and hydrocarbons.
- *Flame retardancy:* Poly(butylene terephthalate), a thermoplastic that is used in electrical connectors even though is flammable. By dispersing nano clay in this polymer, a nanocomposite was produced with improved flame retardant performance.

The objective of this thesis is to investigate a Polyamide-imide (PAI) + Montmorillonite (MMT) nanocomposite. The role of MMT concentration on state of

dispersion was determined using optical microscopy, x-ray diffraction (XRD), Transmission Electron Microscopy (TEM) and Scanning Electron Microscopy (SEM). The influence of MMT concentration on the glass transition (T_g) was determined using Differential Scanning Calorimetry (DSC). The results were correlated to the state of dispersion based on the influence of chain confinement. Since the MMT is treated organically with alkyl ammonium surfactants having a degradation temperature of 270^{o}C, Thermogravimetric Analysis (TGA) was conducted to determine if the high PAI degradation temperature was compromised. Since the end use application of the PAI suspension is in high temperature wire coating, the influence of MMT on the mechanical properties was determined through Vickers hardness measurements. The results indicate that MMT concentration affects the state of dispersion, which has a dominating influence on the glass transition (T_g), degradation and mechanical properties.

Chapter 2

POLYAMIDE-IMIDE (PAI)

PAI is an amorphous polymer, which is injection molded as a thermoplastic and then post cured at elevated temperature to induce condensation polymerization, which results in a thermoset structure with exceptional high temperature capabilities. The polymer is capable of performing under severe stress conditions at continuous temperatures to 260^{o}C[58]. The name amide-imide comes from the presence of amide groups alternately linked with imide groups. Applications for PAI include:

- Rockets, Missiles: JAG antitank missile launcher (nozzle cup), Lockheed Martin Saturn V rocket separators.
- Hydraulic ram seals
- Motors for atomic power stations and space research satellite, motors for hermetic applications, chemical industries, furnaces and motors in radioactive atmospheres.
- Pin straighteners in IC package processing.
- Successful replacement of the metal ball at the tips of the pen by the tough wears resistant PAI ball.
- Due to its resistance towards radiation, PAI is used in nuclear reactors and particle accelerators.

2.1 Characteristics of Polyamide-imide[58]

Exceptional dimensional stability:

Glass transition temperature plays a major role in dimensional stability of all the polymers. Glass transition temperature is a temperature boundary for almost all the amorphous polymers (and many crystalline polymers) above which the polymer remains soft, flexible and rubbery and below which it becomes hard, brittle and glassy. PAI has a glass transition temperature above 275^{o}C. Due to such a high glass transition temperature, PAI has exceptional dimensional stability throughout its operating temperature range.

Wide Range of Temperature Capability:

PAI is functional from the temperature of liquid nitrogen to as high as 260^{o}C. The combination of aromatic groups and imide linkages is responsible for exceptional thermal stability.

Retention of Properties after Thermal Aging:

PAI resists chemical breakdown and retains high strength even after prolonged thermal exposure.

Radiation Stability:

Polyamide-imide is a remarkably stable polymer in radiation environments. This gives polyamide-imide an ability to use in nuclear reactors. PAI is also resistant towards ultraviolet radiation.

Mechanical Strength:

PAI has excellent tensile and flexural strength showing retention of these properties in continuous service at temperatures in excess of 232^{o}C. PAI also has a high modulus making it a good replacement for metals providing equivalent stiffness at significantly lower weight.

Low Coefficient of Thermal Expansion:

The coefficient of thermal expansion of polyamide-imide falls within the same range as that of most structural metals. This is why PAI is used in electronic packaging industry and in wire coating industry.

Outgassing characteristics:

The use of a material in the high vacuum of outer space requires that it not outgas condensable species, which would be deposited on sensitive optical devices, effectively destroying their capabilities. Plastics generally do outgas un-reacted monomers, low molecular weight polymer fractions, plasticizers, stabilizers, and so on. PAI contains none of these. Any volatile that might be present would be effectively removed during the curing step.

Chemical Resistance:

High pH alkaline systems and some oxidizing acids attack polyamide-imide. PAI is also affected by aqueous systems at elevated temperature. Sodium hydroxide, benzene, sulfonic acid, amino-ethanol, and steam above $160^{o}C$ attack polyamide-imide. With these exceptions PAI is generally considered to have excellent chemical resistance properties.

Chapter 3

STRUCTURE AND CHARACTERISCTICS PROPERTIES OF LAYERED SILICATES

Clay minerals belong to the phyllosilicates[52,53,59]. These are two-dimensional arrays of silicon-oxygen tetrahedra and two-dimensional arrays of aluminum or magnesium-oxygen-hydroxyl octahedra.

In the case of silicon-oxygen sheets, silicon atoms are coordinated with four oxygen atoms. The oxygen atoms are located on the four corners of a regular tetrahedron with the silicon atom in the center. This is shown in **Figure 3.1**. In the sheet, three neighboring tetrahedra share three of the four oxygen atoms of each tetrahedron and the fourth oxygen atom of each tetrahedron is pointed downward as shown in **Figure 3.2**. The silicon-oxygen sheet is called the tetrahedral sheet or the silica sheet[59].

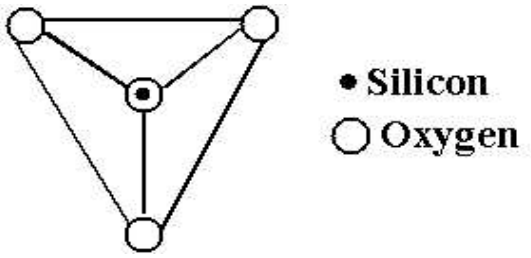

Figure 3.1 Tetrahedral arrangement of Si and O[53]

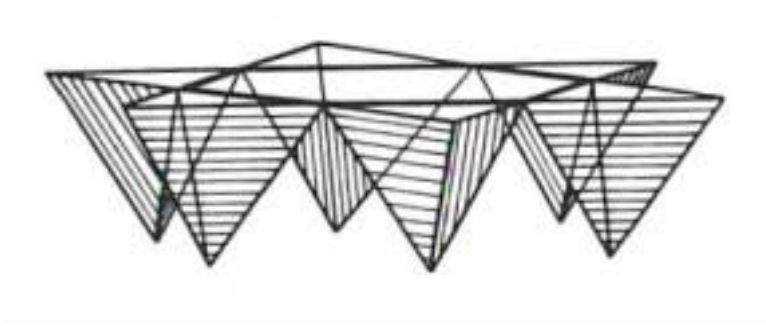

Figure 3.2 Perspective sketch of tetrahedral linking[59]

In case of Al-, Mg-O-OH sheets, the Al or Mg atoms are coordinated with six oxygen atoms or OH groups. A regular octahedron is formed with the corners occupied by oxygen or OH groups and Al or Mg at the center. This is shown in **Figure 3.3**. Sharing of oxygen or OH groups with a neighboring octahedron result in a sheet structure which is shown in **Figure 3.4**. The sheet is called octahedral sheet or the alumina or magnesia sheet[59].

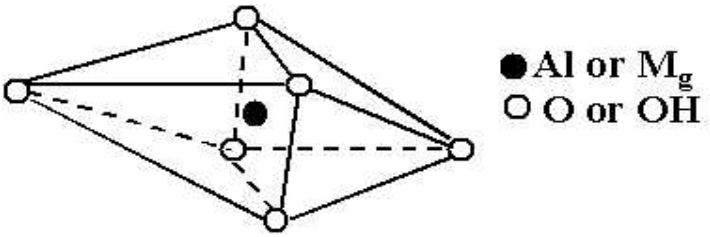

Figure 3.3 Octahedral arrangement of Al or Mg with O or OH[53]

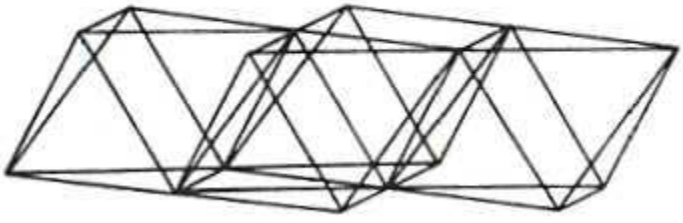

Figure 3.4 Perspective sketch of octahedral linking[59]

The tetrahedral and octahedral sheets have similar symmetry and identical dimensions. This helps in the sharing of oxygen atoms between these sheets. Thus the octahedral sheet shares the fourth protruding oxygen atom from tetrahedral sheet. If the sharing occur between one silica and one alumina sheet, it is called 1:1 layer minerals and if one alumina sheet shares two oxygen atoms from silica sheets, it is called 2:1 layered mineral. Within each layer there is a repetition of structure and therefore it is referred as a unit cell. The distance between a certain plane in the layer and the corresponding plane in the next layer is called the basal or d spacing. The basal spacing can be determined by XRD. The basal spacing is around $7.2A^{o}$ in 1:1 layer clays and $9.2A^{o}$ in 2:1 layer clays. The bonding between the layers is weak (van der Waals type) but a strong covalent bond exists between the atoms of the same layer[52,53,59].

There are three principle groups of phyllosilicates, montmorillonite, illite and kaolinite. Montmorillonite has 2:1 layered structure, illite has 2:1 layered structure and kaolinite has 1:1 layered structure[59].

3.1 Montmorillonite

The suggested crystallographic structure for mica type layered silicate is shown in **Figure 3.5**.

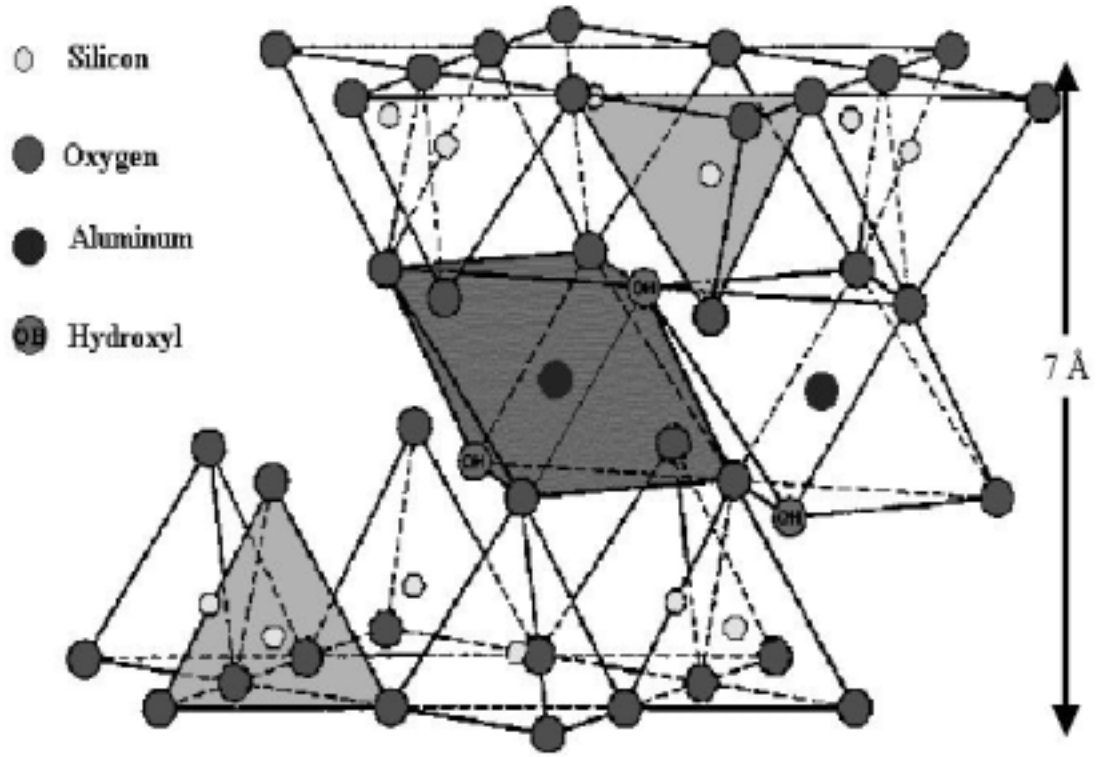

Figure 3.5 Suggested layered structure of mica type layered silicates[52, 53]

This structure is derived from pyrophyllite and talc by substitution of certain atoms for other atoms. In the tetrahedral sheet, Si^{4+} replaces Al^{3+}. In octahedral sheet, Al^{3+} replaces $Mg2^{+}$. The substitution of higher valence atoms results in a deficit of positive charge or excess of negative charge. The excess of negative charge within the layers is balanced by adsorption of cations. These clays which are hydrophilic in nature have Na^{+}, K^{+} or Ca^{2+} cations in the layer gallery.

Mica-type layered silicates (MTSs) are distinguished by the location and type of cations in the layer. **Table 3.1** summarizes the classification of MTSs.

Table 3.1 Classification of Montmorillonoids[59]

Principal Substitutions	Trioctahedral Minerals	Dioctahedral Minerals
Prototype (no substitutions)	Talc	Pyrophyllite
	Mg_3Si_4	Al_2Si_4
All Octahedral	Hectorite	Montmorillonite
	$(Mg_{3-x}Li_x)(Si_4)$	$(Al_{2-x}Mg_x)(Si_4)$
Predominantly Octahedral	Saponite	Volchonskoite
	$(Mg_{3-x}Al_x)(Si_{4-y}Al_y)$	$(Al, Cr)_2(Si_{4-y}Al_y)$
	Sauconite	
	$(Zn_{3-x}Al_x)(Si_{4-y}Al_y)$	
Predominantly Tetrahedral	Vermiculite	Nontronite
	$(Mg_{3-x}Fe_x)(Si_3Al)$	$(Al,Fe)_2(Si_{4-y}Al_y)$

Due to high concentration of negative charge, the surface oxygens of tetrahedrally substituted MTS are strong electron donors than the surface oxygens of octahedrally substituted MTS.

3.2 Surface treatment of clay minerals[52]

Clay is hydrophilic by nature. This hydrophilic nature can affect the miscibility of clay with an organophilic polymer. Therefore the surface of the clay is treated to make it hydrophobic and more organophilic. This is a cation exchange reaction where inorganic cations such as Ca^{2+}, K^+ and Na^+ are replaced by organically modified cations, such as alkyl ammonium ($R\text{-}NH_3^+$) groups. R is long aliphatic residue. The cationic head of the

aliphatic group is found close to the surface layer due to the presence of negative charge on the layer and the tail without charge is found away from the layer. Four types of structures are possible depending on the packing density, temperature and chain length of the aliphatic groups. These are shown in **Figure 3.6-3.9**. When the alkyl ammonium chains lie parallel to the host layers a lateral monolayer or lateral bilayer is formed. If alkyl ammonium chains radiate away from the host layers, an extended paraffin-type monolayer or paraffin-type bilayer structure is formed.

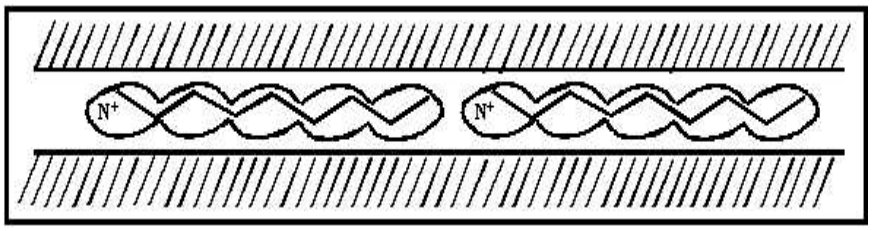

Figure 3.6 Lateral monolayer[52]

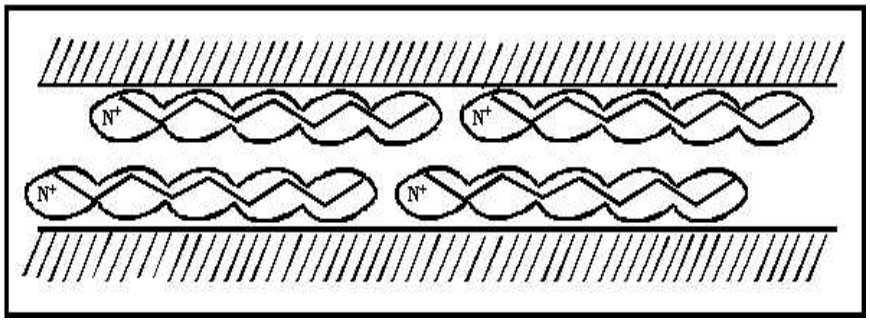

Figure 3.7 Lateral bilayer[52]

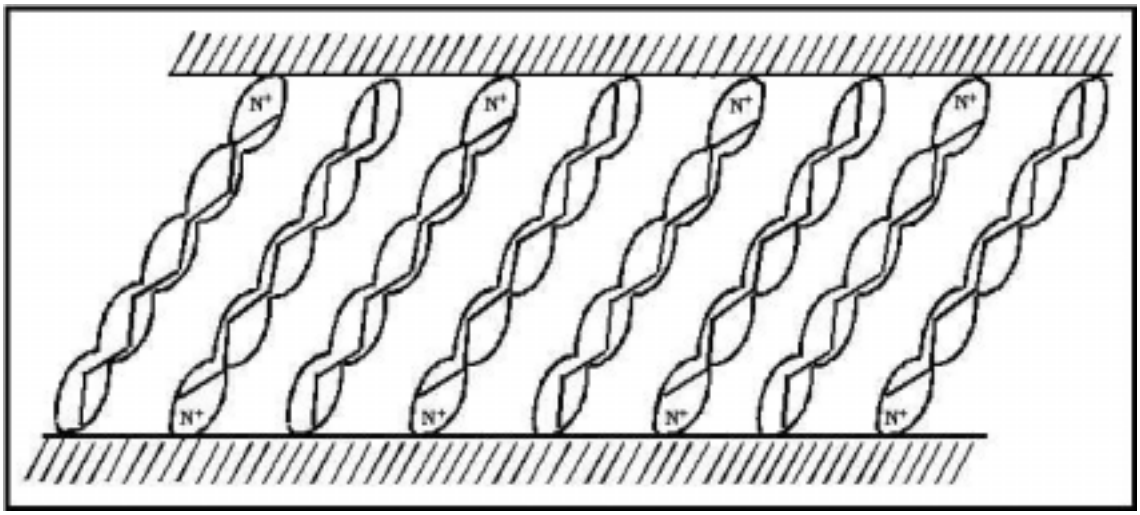

Figure 3.8 Paraffin type monolayer[52]

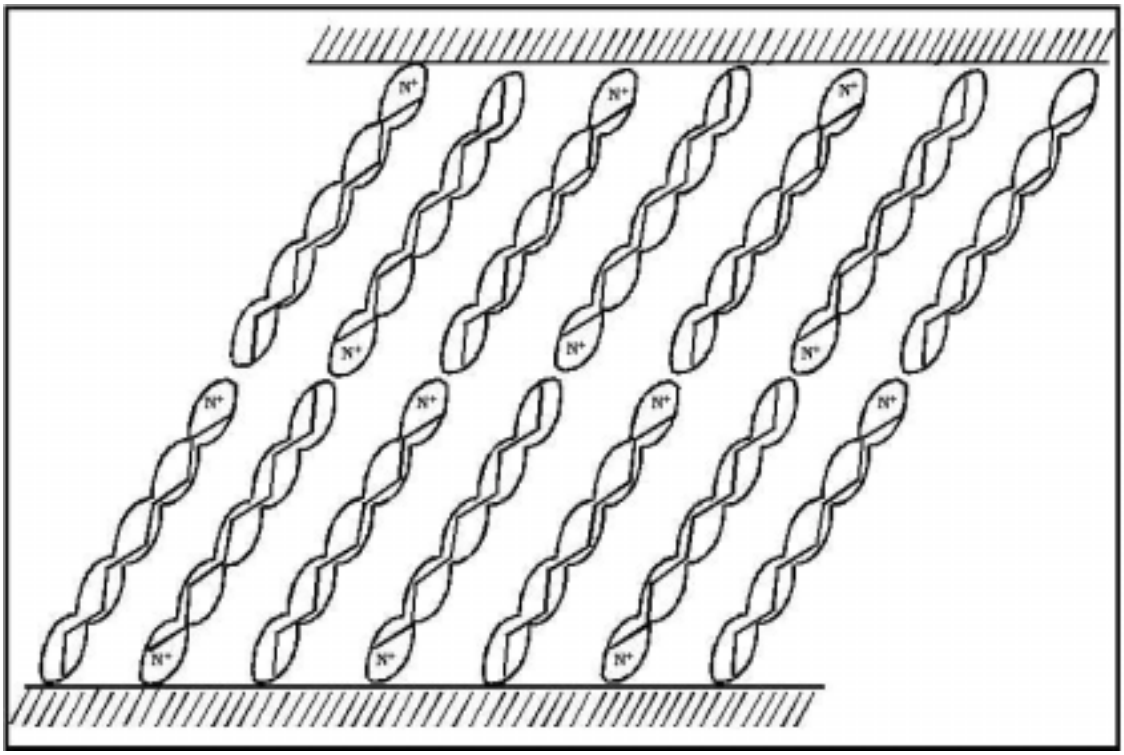

Figure 3.9 Paraffin type bilayer[52]

Vaia and his colleagues developed a schematic structure model for the organically modified fluorohectorite (FH-C_n). The schematic structure of a model is shown in **Figure 3.10-3.12**. Fourier transform infrared spectroscopy (FTIR) along with x-ray diffraction was used to investigate the model. By monitoring the frequency shifts of the asymmetric CH_2 stretching and bending vibrations, they found that the alkyl ammonium chains exist in states with varying degrees of order. Depending upon the number of carbon atoms present in an alkyl ammonium chain, the model adopts a more ordered structure. For the least number of carbon atom i.e. when the chain is short, the molecules are isolated from each other, which is shown in **Figure 3.10**. In **Figure 3.11** for intermediate chain lengths, a structure with varying degree of in-plane disorder is formed. At higher chain lengths, an increase in interlayer order was determined, which is shown in **Figure 3.12**. Thus as the interlayer packing density increases, the alkyl ammonium chains adopt a more disordered structure.

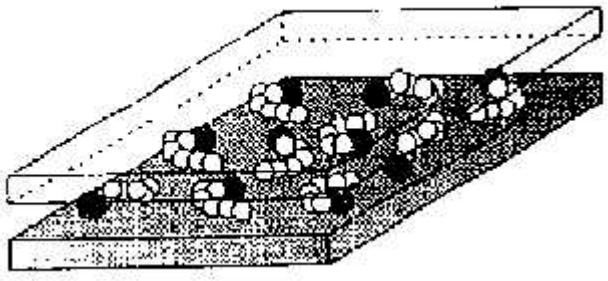

Figure 3.10 Alkyl chain aggregation model for the shortest lengths of carbon atoms (Open circles represent CH_2 segments while filled circles represent cationic head groups)[52]

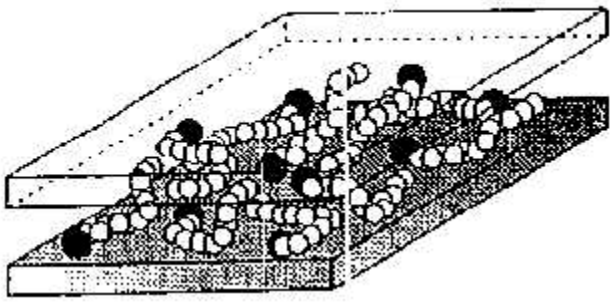

Figure 3.11 Alkyl chain aggregation model for the intermediate lengths of carbon atoms (Open circles represent CH_2 segments while filled circles represent cationic head groups)[52]

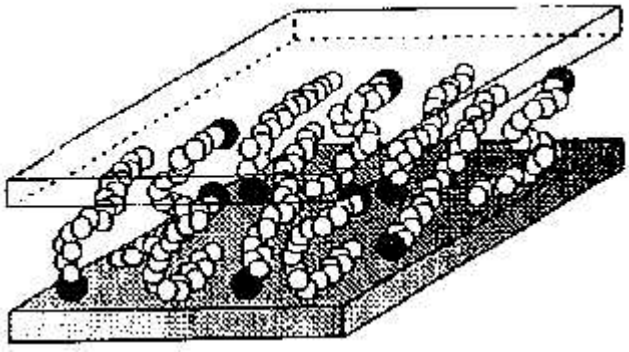

Figure 3.12 Alkyl chain aggregation model for the longer lengths of carbon atoms (Open circles represent CH_2 segments while filled circles represent cationic head groups)[52]

The alkyl ammonium chains in the galleries make clay organophilic. Surface energy of the layered silicates is reduced due to the presence of alkyl ammonium chains thus allowing organic species with varying degrees of polarities to intercalate between the layers.

3.3 Dispersions of Clay in a Nanocomposite[1-26,52,54]

In considering particulate reinforced polymer composite an important parameter is the dispersion of reinforcement. Uniform dispersion is key to better mechanical and thermal properties.

The addition of clay in a host matrix produces three different types of dispersions.

- Intercalated dispersion
- Exfoliated dispersion
- Immiscible dispersion

Figure 3.13 shows an intercalated dispersion. As the **Figure 3.13** indicates a finite penetration of polymer chains into silicate galleries result in the finite expansion of silicate galleries. A well-ordered multi layered structure with retention of clay structure is obtained.

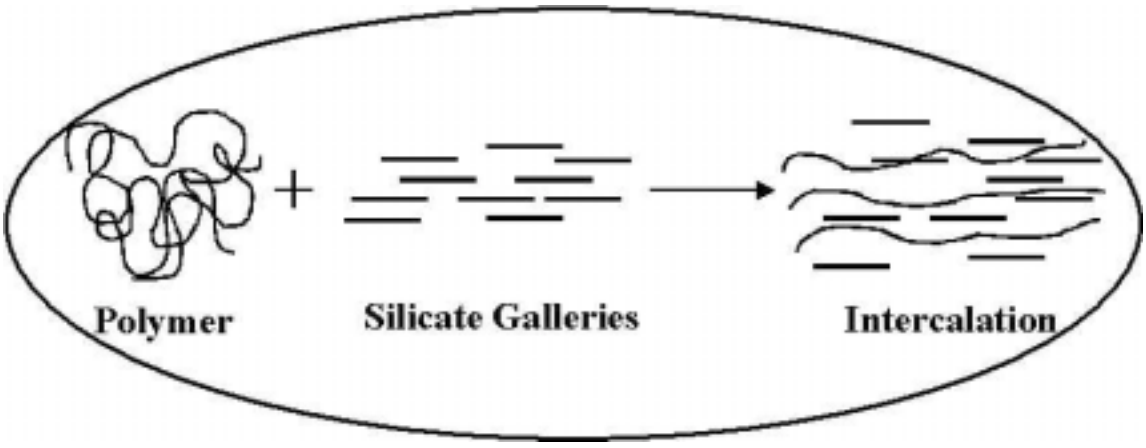

Figure 3.13 Intercalated dispersion of polymer nanocomposites

Extensive penetration of polymer chains into silicate galleries, which result in disorder and eventual delamination with a complete disruption of clay structure, is called as exfoliated dispersion. Exfoliated dispersion is shown in **Figure 3.14**.

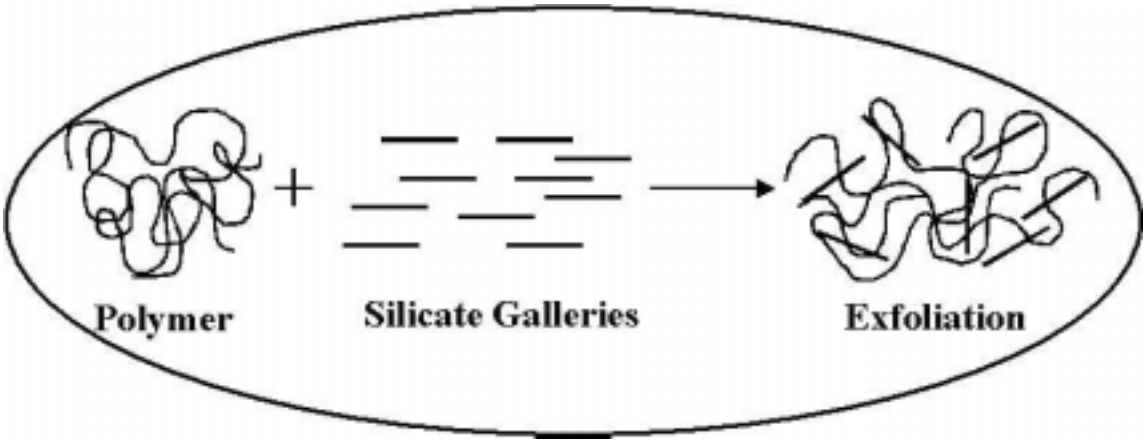

Figure 3.14 Exfoliated dispersion in polymer nanocomposites

Immiscible or macro system represents complete immiscibility of clay and polymer on the molecular level. Both clay and polymer retain their individual identities without affecting their structure. This effect is shown in **Figure 3.15**.

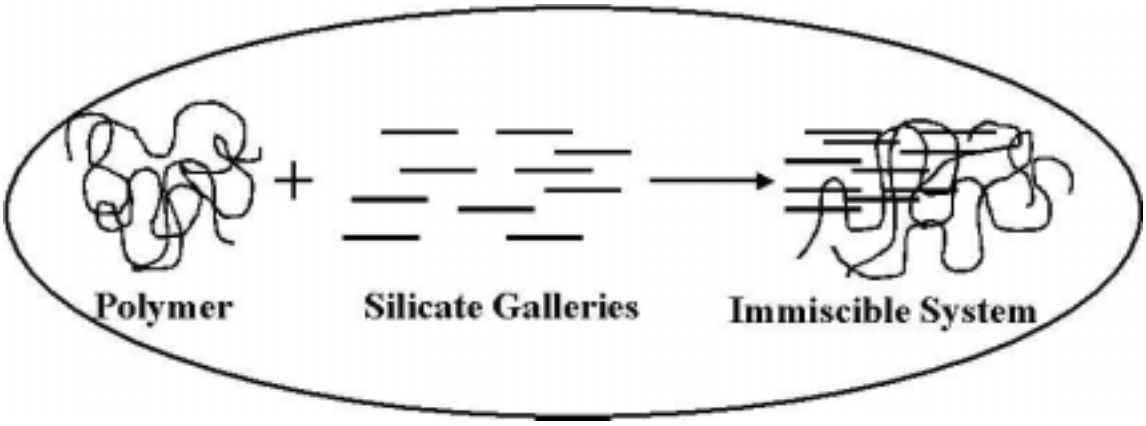

Figure 3.15 Immiscible or macro dispersion in polymer nanocomposites

The question that comes to the mind is what kind of dispersion can one expect in a given polymer and clay system. The factors, which affect the dispersion and miscibility in a polymer clay nanocomposites, are as follows

- Packing density of clays.
- Chain length of organic cations.
- Charge on the layer.
- Processing temperature.
- Shear during nanocomposite formation.
- Type of bonding at polymer/silicate interface.
- Polymer-polymer, polymer-silicate & silicate-silicate interaction.

3.4 Synthesis of Polymer Clay Nanocomposites[54]

There are three methods to prepare a polymer clay nanocomposite

- In-Situ Polymerization
- Polymer Solution Intercalation
- Melt Intercalation

3.4.1 In-Situ Polymerization

This was the first method used to synthesize polymer clay nanocomposite. The first polymer used was nylon (polyamide 6). Nowadays this is a common method for thermoset nanocomposites.

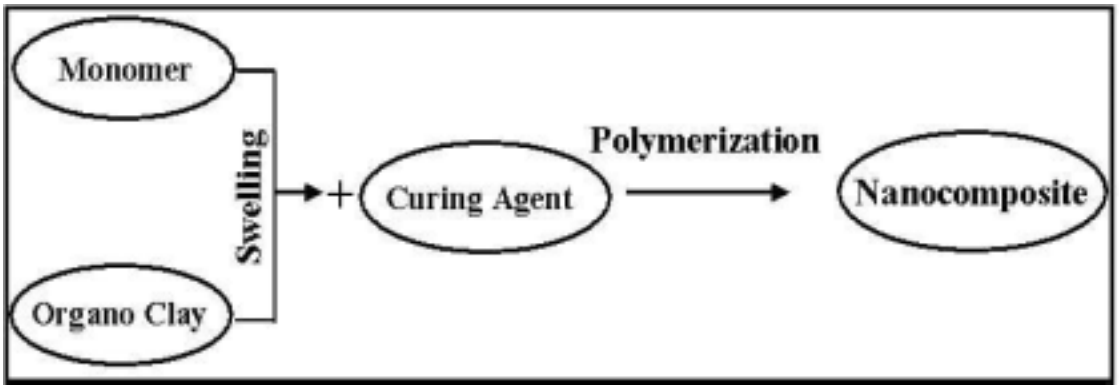

Figure 3.16 Flow chart of the "in-situ polymerization" approach[54]

Figure 3.16 is a flow chart showing various steps involved in in-situ polymerization. The first step is to achieve the swelling of organoclay in monomer. This is a time consuming step since the swelling depends on the polarity of monomer molecules, surface treatment of clay and swelling temperature. Then depending upon the type of polymer, the reaction is initiated. In case of thermoplastics, the polymerization is achieved by addition of free radicals or by an increase in temperature. In case of thermosets, a curing agent is added to initiate polymerization.

The driving force for this "in situ-polymerization" depends on the polarity of monomer molecules. Due to high surface energy of the clay, monomer molecules get diffused between the clay layers. The diffusion is continued till equilibrium is reached. During polymerization, monomer starts to react with the curing agent or free radical. This reaction lowers the overall polarity of the intercalated molecules so that more polar molecules are driven between the clay layers. The overall reaction is shown in **Figure 3.17**. The most important thing is to control the polymerization occurring between the layers (intragallery polymerization). If the cure kinetic is lowered between the layers than outside the layers (extragallery polymerization), delamination of clay is possible.

Therefore greater importance is given to intragallery polymerization than to extragallery polymerization.

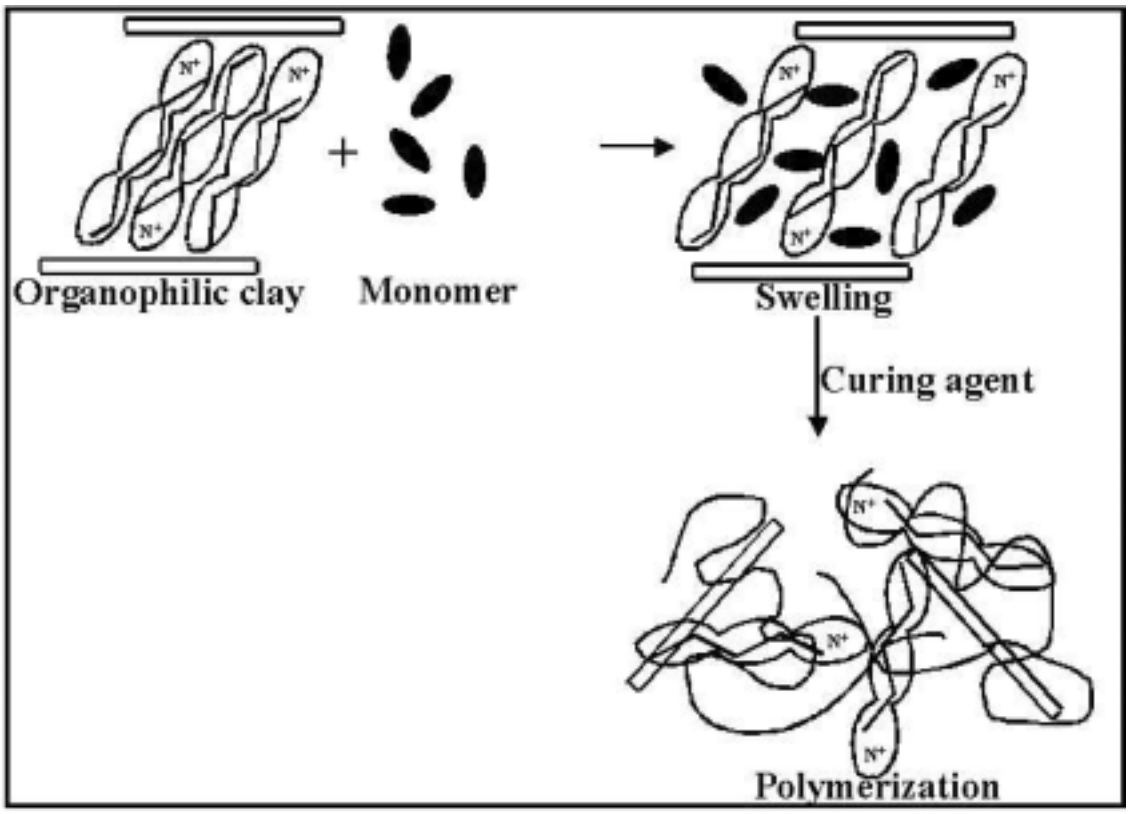

Figure 3.17 Chemical steps involved in the "in-situ polymerization"[54]

This synthesis method allows control of the molecular weight of the polymer and the distribution of molecular weights. Since the polymer growth process is one known as "living polymerization", it allows for additional monomers to be added to grow block copolymers. But the method is limited to polymers that can be grown by living polymerization.

3.4.2 Polymer Solution Intercalation

This method is different from the "in-situ polymerization" is that it makes the use of a preformed polymer instead of monomer (**Figure 3.18**). Polymer solution

intercalation is based on a solvent system in which the polymer is soluble and the silicate layers are swellable. The first step is the swelling of clay in a solvent usually a polar solvent (**Figure 3.18**). Then the polymer, dissolved in the solvent is added to the solution and intercalates between the clay layers. The last step is the removal of solvent by evaporation normally under vacuum. After solvent removal, the intercalated structure remains.

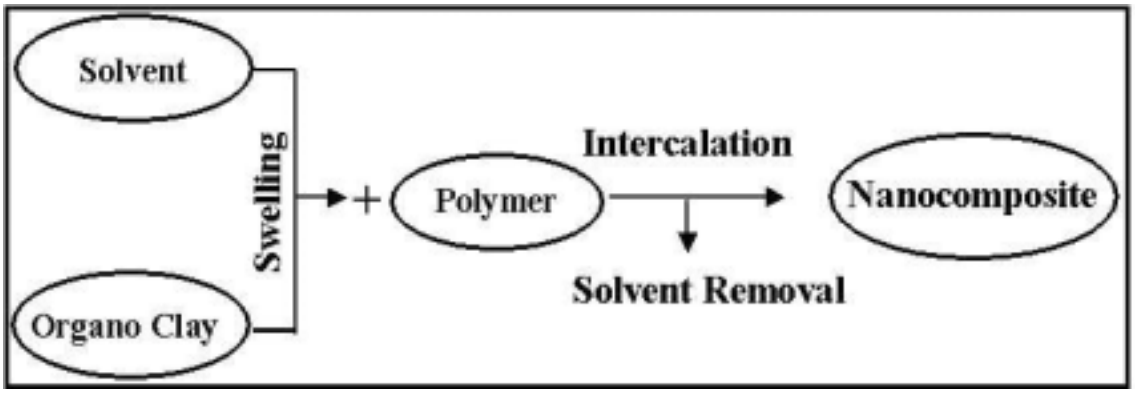

Figure 3.18 Flow chart of the "solution" approach[54]

The driving force for polymer solution intercalation is the entropy gained by desorption of solvent molecules, which compensates for the decrease in conformational entropy of the intercalated polymer chains. Therefore, a relatively large number of solvent molecules need to be desorbed from the clay to accommodate the incoming polymer chains. The advantage of this method is that it offers the possibility of synthesizing intercalated nanocomposites based on polymers with low or no polarity.

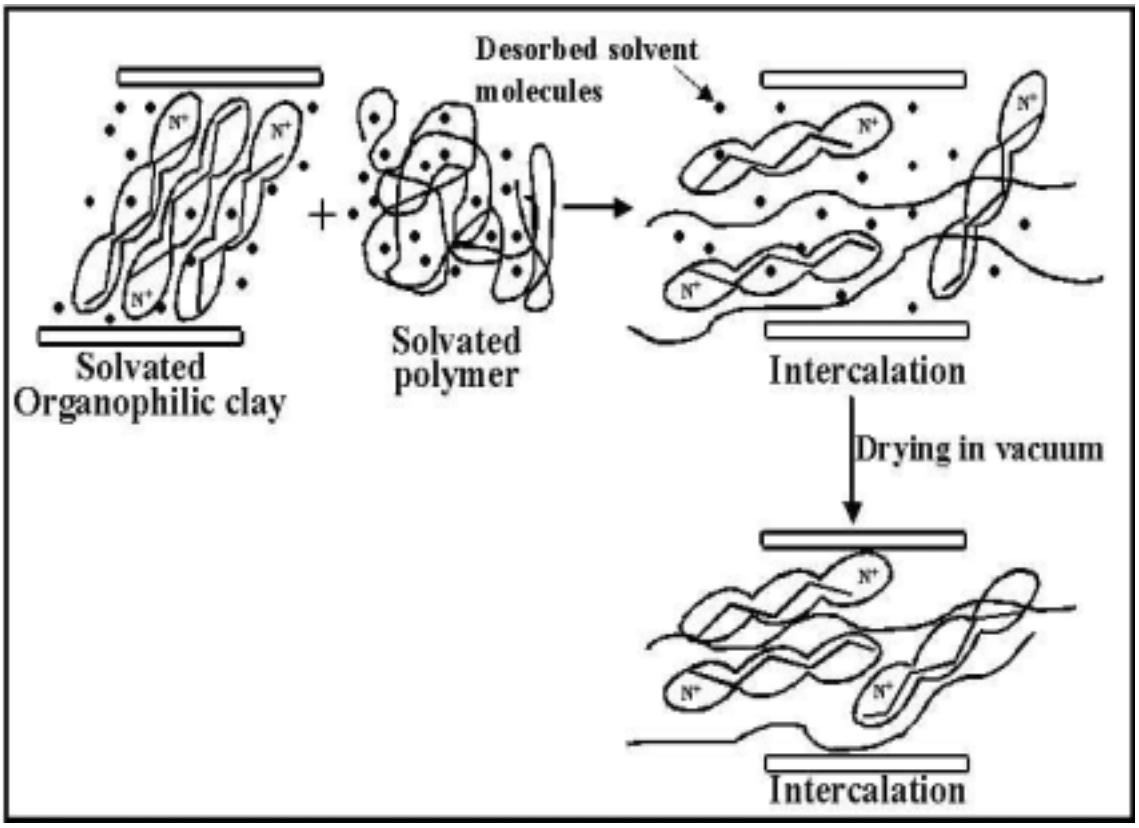

Figure 3.19 Intercalation of the polymer by the "solution" approach[54]

The water soluble polymers, which have been used to make nanocomposites by this technique are poly(vinyl alcohol), poly(vinyl pyrrolidione), poly(ethylene oxide), poly(ethylene vinyl alcohol) and linear poly(ethylenimine) using water as the solvent.

3.4.3 Melt Intercalation

In 1993 Vaia and his colleagues were the first to report melt intercalation. This method is used to make thermoplastic nanocomposites and the method is not applicable for thermosets because the process involves the melting of a polymer. The process involves blending of a molten thermoplastic with organoclay and then annealing at a temperature above the glass transition temperature of the polymer. The mechanism is shown in **Figure 3.20 and 3.21**.

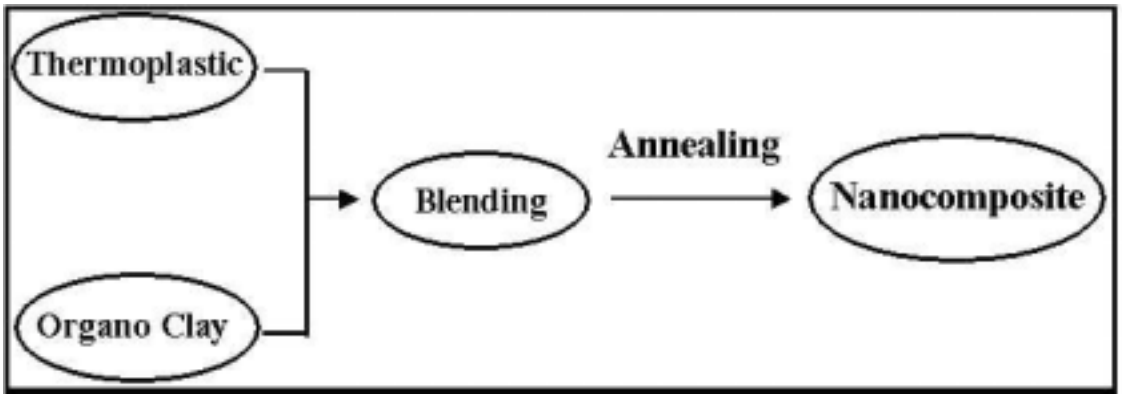

Figure 3.20 Flow chart of the "melt intercalation" approach[54]

The observation that polymer chains can undergo center of mass diffusion in essentially two dimensions is rather surprising because the unperturbed chain diameters (10nm) are approximately an order of magnitude greater than the interlayer distance between the silicate sheets (1nm).

The proposed driving force for this mechanism is the important enthalpic contribution of the polymer-clay interactions during the blending and annealing steps.

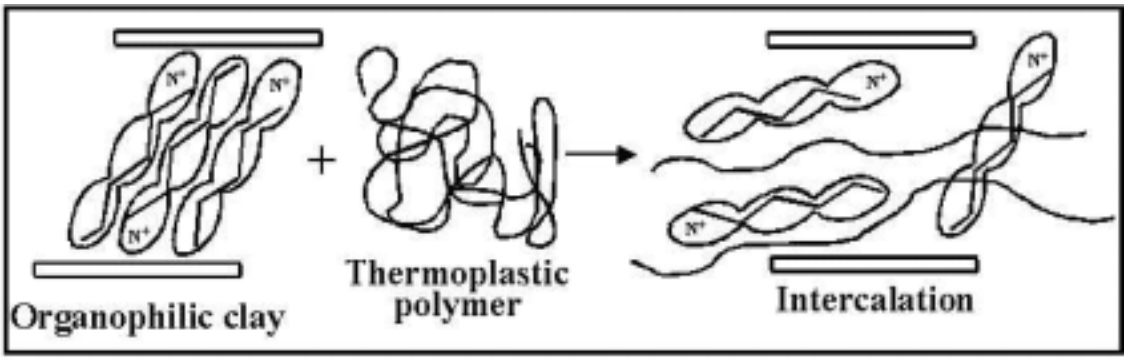

Figure 3.21 Chemical steps involved in "melt intercalation" approach[54]

Since the process involves the blending of polymer with clay, melt intercalation is one of the most popular methods to prepare nanocomposites in industry. Different

thermoplastics have been tried so far to make nanocomposites by this technique, e.g. polypropylene, polyethylene, nylon, polystyrene.

Chapter 4

EXPERIMENTAL

To investigate the PAI + montmorillonite nanocomposite, experiments were designed to resolve the following issues:

1. The potential for MMT to form an intercalated or exfoliated nanocomposite with PAI
2. The influence that MMT had on the glass transition temperature of PAI
3. Retention of high thermal stability of PAI
4. Improved surface hardness of the nanocomposite due to MMT addition.

4.1 Sample Preparation

P.D. GEORGE CO. supplied PAI in the form of suspension (oligomer). Development of process technology is an important step in nanocomposites because dispersion of the clay depends upon effective process technology. Two techniques were tried to develop PAI nanocomposites. Southern Clay products provided Cloisite 20A and untreated MMT (Cloisite Na).

4.1.1 Spinning Technique

Clay was premixed with xylene to improve its wetting ability towards the PAI suspension and increase effect of swelling. Xylene was chosen as a swelling solvent because of his presence in PAI suspension. This premixed solution of xylene and clay was added to PAI suspension. A high-speed spinner was used to cast a film of PAI nanocomposite on glass and on a Teflon surface. Controlling the speed and time of

spinning, films of various thicknesses were obtained. Films were cured in an mechanical convection oven at 175^{o}C for 4 hours.

There were few disadvantages of this method

- Very thin samples were obtained but not thin enough for TEM.
- After curing PAI sticks to surface of glass and Teflon, pilling of film was difficult.
- Due to drawback of pilling, difficult to achieve big sections of films.
- Yield percentage was very less.

4.1.2 Casting Technique

To overcome the problems encountered by the spinning technique and to develop a processing technology capable of industrial application, a casting technique was developed. Silicone molds were prepared of known different size and shape. Clay was premixed with xylene for 1hour to improve its swelling capacity. The solution of premixed and xylene was added very slowly into PAI suspension. The suspension was stirred continuously with the help of a Caframo BDC1850 digital mechanical stirrer with a stepwise increase in stirring speeds ranging from 50rpm to 800rpm. The high rpm prevented the flocculation of clay particles.

Samples were cured in a mechanical convection oven. PAI suspension was a mixture of PAI oligomer plus four different aromatic hydrocarbon solvents. A selective solvent evaporation technique was used to decrease the effect of trapping of solvents inside or warpage. Sample were cured between 30^{o}C and 175^{o}C. The temperature of the oven was increased by 10^{o}C after every 1.5hours until the final temperature was reached. This technique gave bulk samples as well as thin films with controlled size and shape.

Five different compositions (1.0, 1.5, 2.0, 2.5 and 3.0% by weight percent of PAI) of PAI + MMT were prepared. Clay was taken according to weight percent of PAI. Thin films of uniform thickness were used for XRD, optical microscopy, SEM & hardness testing. Thin sections of bulk samples were used for TEM.

4.2 Microstructural Analysis

Polarizing optical microscopy, XRD, TEM and SEM were used for microstructural analysis.

4.2.1 Polarizing Optical Microscopy

The light optical microscope enables us to directly view structures that are below the resolving power of the human eye (0.1mm)[60].

Optical microscopy was conducted on a Zeiss polarizing optical microscope. The lens magnification was 40X. The pictures were taken using CONTAX camera. The characteristics of materials that may be determined with the polarized light microscope are morphology, size, transparency or opacity, color, melting point, eutectics, extinction angle, degree of crystallinity etc.[60]

4.2.2 X-ray Diffraction (XRD)

X-ray diffraction (XRD) is a powerful technique used to uniquely identify the crystalline phases present in materials and to measure the structural properties (strain state, grain size, epitaxy, phase composition, preferred orientation and defect structure) of these phases. XRD is also used to determine the thickness of thin film and multilayers and atomic arrangements in amorphous materials (including polymers) and at interfaces. XRD offers unparalleled accuracy in the measurements of atomic spacing and is the

technique of choice for determining strain states in thin films. XRD is a non-contact and nondestructive technique, which makes it ideal for in situ studies[61].

X-rays are high-energy electromagnetic radiation. They have energies ranging from about 200eV to 1 MeV, which puts them between γ-rays and ultraviolet (UV) radiation in the electromagnetic spectrum. When an atom is excited by removal of an electron from an inner shell, it usually returns to its normal state by transferring an electron from some outer shell to the inner shell with consequent emission of energy as X rays[62].

X-rays can be used in chemical analysis in three different ways emission analysis, absorption analysis and diffraction analysis. The emission analysis uses the fact that the x-rays emitted by an excited element have a wavelength characteristic of that element and intensity proportional to the number of excited atoms. Thus emission analysis can be used for both qualitative and quantitative analysis. The absorption analysis utilizes the fact of differing absorption of x-rays by different materials. The diffraction analysis is based on diffraction of x-rays from the planes of a crystal. This method depends upon the wave character of x-rays and the regular spacing of planes in a crystal. We have made use of diffraction analysis for the nanocomposites.

In 1912 a German physicist Von Laue reasoned that, crystals were composed of regularly spaced atoms which might act as scattering centers for x-rays. Because x-rays are electromagnetic waves of wavelength about equal to interatomic distance in crystals, it should be possible to diffract x-rays by means of crystals.

Two English physicists, W. H. Bragg and his son W. L. Bragg successfully analyzed the laue experiment and were able to express the necessary conditions for diffraction in a considerably simpler mathematical form. W. L. Bragg formulated a relationship between the wavelength of x-ray, the pacing between the atomic planes and the diffraction angle.

$$n\lambda = 2d \sin\Theta \qquad \text{(Eq. 4.1)}$$

Where, n = order of reflection

λ = wavelength of x-ray

d = spacing between atomic planes

$\sin\Theta$ = diffraction angle

This relation is known as Bragg's law. It states the essential condition, which must be met if diffraction is to occur[62].

A Siemens D500 X-ray Diffractometer was used to study the diffraction behavior of clay composites. All the experiments were carried out between 2Θ equal to 2^o to 40^o. The scanning speed was 1^o/min and the step speed was 0.05^o. Thin film samples of average thickness equal to 400-500 microns were used. Experiments were carried out at room temperature. The basal spacing or the d spacing was calculated by using Bragg's equation (4.1).

4.2.3 Transmission Electron Microscopy (TEM)

Dispersion of clay in a nanocomposite is one of the most important parameters, which determines the final properties of the nanocomposite. Transmission electron

microscopy is a powerful technique helping us to study the structures at very high magnification scale. Therefore, TEM can be used to support the results obtained from x-ray diffraction. In TEM we can see the distribution of clay platelets and can even find the average distance between the clay platelets. Therefore, TEM is used extensively to study the dispersion behavior of clay in polymer clay nanocomposites.

TEM provides a high lateral spatial resolution. In TEM, a focused electron beam is incident on a thin film (less than 200nm) sample. The signal in TEM is obtained from both un-deflected and deflected electrons that penetrate the sample thickness. A series of magnetic lenses at and below the sample position are responsible for delivering the signal to a detector. Accompanying this signal transmission is a magnification of the spatial information in the signal by as little as 50 times to as much as a factor of 10^6. This remarkable magnification range is facilitated by the small wavelength of the incident electrons, and is the key to the unique capabilities associated with TEM analysis[63].

The TEM study was conducted on a JEOL JEM-100CX II electron microscope. A MT6000 Sorvall microtome was used to cut the thin sections of the sample.

Thin sections of polymer nanocomposite (less than 100nm thick) were cut on a Sorvall microtome machine. A small sliver (15-20mg) of sample was embedded in a liquid epoxy. The epoxy was cured and provided the support to PAI nanocomposite. Samples were cut using diamond knife and the floating thin films on the water surface were collected on grids and dried at room temperature.

4.2.4 Scanning Electron Microscopy (SEM)

The scanning electron microscope (SEM) is the most widely used form of electron microscope in the field of materials science. The SEM is popular because it uniquely combines some of the simplicity and ease of specimen preparation of optical microscopy with much of the performance capability and flexibility of the more expensive and complex transmission electron microscope. The SEM provides the investigator with a highly magnified image of the surface of a material that is very similar to what one would expect if one could actually see the surface visually.

The SEM is a microscope that uses electrons rather than light to form an image. There are many advantages of SEM over light microscopy. The SEM has a large depth of field, which allows a large amount of the sample to be in focus at one time. The SEM also produces images of high resolution, which means that closely spaced features can be examined at a high magnification. Preparation of the samples is relatively easy since most SEM's require only samples to be conductive. The combination of higher magnification, larger depth of focus, greater resolution and ease of sample observation makes the SEM one of the most heavily used instrument in research areas today[64].

Microstructural features were examined using a JEOL T300 scanning electron microscope with 25 kV accelerating voltage and 30mm working distance and spot size of 10. The samples were prepared by fracturing the surface of PAI nanocomposite and were gold sputter coated for electron conductivity.

4.3 Thermal Analysis

DSC was used to study the effect of MMT on T_g of PAI. TGA was used to study the degradation properties of PAI nanocomposites.

4.3.1 Differential Scanning Calorimetry (DSC)

The technique of differential scanning calorimetry (DSC) involves the amount of heat that has to be supplied to establish a zero temperature difference between the sample and an inert reference material against either time or temperature as each specimen is subjected to an identical temperature program. This recorded heat flow gives a measure of the amount of energy absorbed or evolved in a particular transition, and hence gives calorimetric measurements directly. Temperature changes in the sample are due to endothermic or exothermic enthalpic transitions or reactions such as those caused by phase changes, fusion, crystalline structure inversions, boiling, sublimation, vaporization, dehydration, decomposition, oxidation and reduction reactions.

In DSC the sample (S) and reference (R) materials are provided with their own separate heaters, as well as their own temperature sensors. So in DSC both S and R are maintained at identical temperatures by controlling electrically the rate at which heat is transferred to them. The area under the peak in DSC profile is proportional to the heat change involved[65].

The DSC data was obtained on a Perkin-Elmer DSC 7 instrument, which operates in the power compensation mode. The system was calibrated using elemental indium. 5-12 mg of sample was used for each run. A first heating run was carried from 30^{o}C to 400^{o}C at the heating rate of 10^{o}C/min. The sample was held at 400^{0}C for 5 minutes and

then cooled to 30^{o}C at a cooling rate of 10^{o}C/min. The second scan was from 30^{o}C to 400^{o}C at heating rate of 10^{o}C/min.

4.3.2 Thermogravimetric Analysis (TGA)

Thermogravimetric analysis (TGA) is a branch of thermal analysis, which examines the mass change of a sample as a function of temperature in the scanning mode or as a function of time in the isothermal mode. Thermal events like melting, crystallization or glass transition do not change the mass of the sample but there are some very important exceptions which include desorption, absorption, sublimation, vaporization, oxidation, reduction and decomposition. TGA is used to characterize the decomposition and thermal stability of materials under variety of conditions and to examine the kinetics of the physico-chemical processes occurring in the sample. The mass change characteristics of a material are strongly dependent on the experimental conditions. Factors such as sample mass, volume, shape and nature of sample holder, nature and pressure of the atmosphere in the sample chamber and the scanning rate all have important influences on the characteristics of the recorded TGA curve.

TGA is useful to distinguish one polymer from the other on the basis of oxidation or decomposition curves. TGA technique is used to compare the behavior of polymer with and without additives[66].

TGA was performed on Perkin Elmer TGA instrument. The experiments were carried out from 50^{o}C to 1000^{o}C at scanning rate of 20^{o}C/min. The experiments were performed under an air blanket.

4.4 Mechanical Properties

Micro-hardness indentation was used to find out Vickers hardness of PAI nanocomposites.

4.4.1 Microhardness Testing

In general hardness usually implies a resistance to deformation. There are three general types of hardness measurements depending on the manner in which the test is conducted. These are 1) scratch hardness, 2) indentation hardness and 3) rebound or dynamic hardness. Scratch hardness is of primary interest to mineralogists. Indention hardness most likely means the resistance to indentation. In dynamic hardness measurements the indenter is usually dropped onto the material surface[67].

The Vickers hardness test uses a square base diamond pyramid as the indenter. The included angle between opposite faces of the pyramid is 136^{o}. The Vickers hardness (VHN) number is defined as the load divided by the surface area of the indentation. In practice this area is calculated from microscopic measurements of the lengths of the diagonals of the impression[67].

$$VHN = [2PSin(\theta / 2)] / L^{2} \qquad \text{(Eq. 4.2)}$$

Where P = applied load. Kg

L = average length of diagonals, mm

θ = angle between opposite faces of diamond, 136^{o}

The Vickers hardness test has received fairly wide acceptance for research work because it provides a continuous scale of hardness, for a given load, from very soft metals with a VHN of 5 to extremely hard materials with a VHN of 1500.

Experiments for the micro hardness test were carried out on a FM-7 Future Tech Corp. digital, micro hardness tester. Constant load of 300gm was applied. 15 sec of dwell time was chosen for all samples.

Chapter 5

RESULTS AND DISCUSSIONS

5.1 Type of Clay

Two types of clays were used namely Cloisite Na^+ and cloisite 20A. PAI is an organophilic polymer. Cloisite Na^+ is hydrophilic clay and can be used with systems, which are also hydrophilic. Previously people have used cloisite Na^+ with water-soluble polymer[12]. Optical microscopy and x-ray diffraction techniques were used to study the difference in dispersion of clays in PAI.

Figure 5.1-5.4 is a comparison of optical micrograph of 1.0% and 3.0% (by weight) cloisite Na^+ + PAI nanocomposite with 1.0% and 3.0% (by weight) cloisite 20A + PAI nanocomposite. The magnification for all the optical micrographs was 40X.

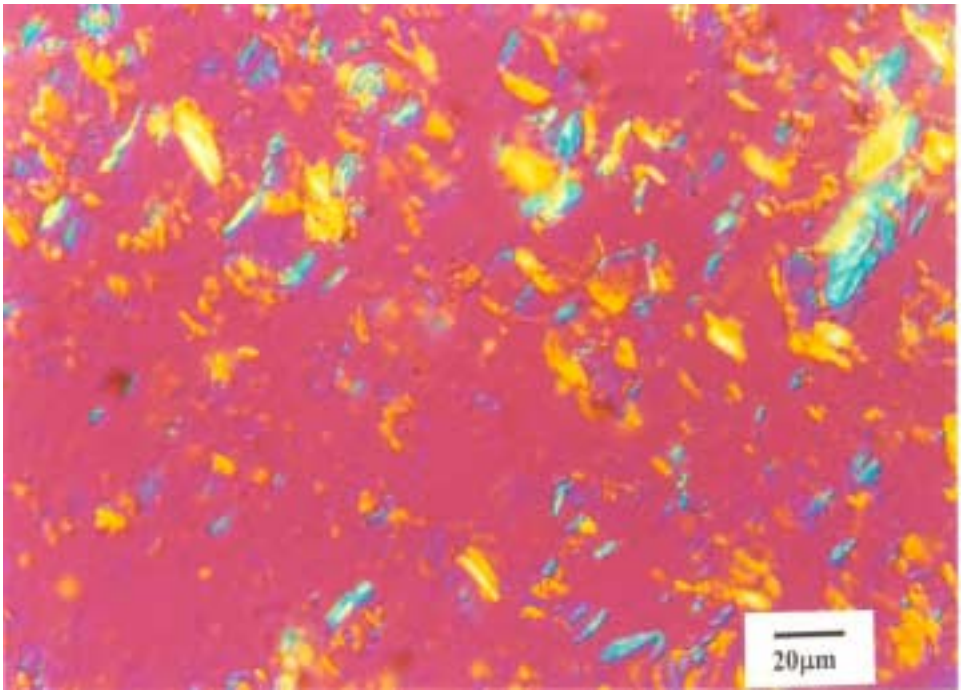

Figure 5.1 Optical micrograph of 1.0% cloisite Na^+ + PAI nanocomposite

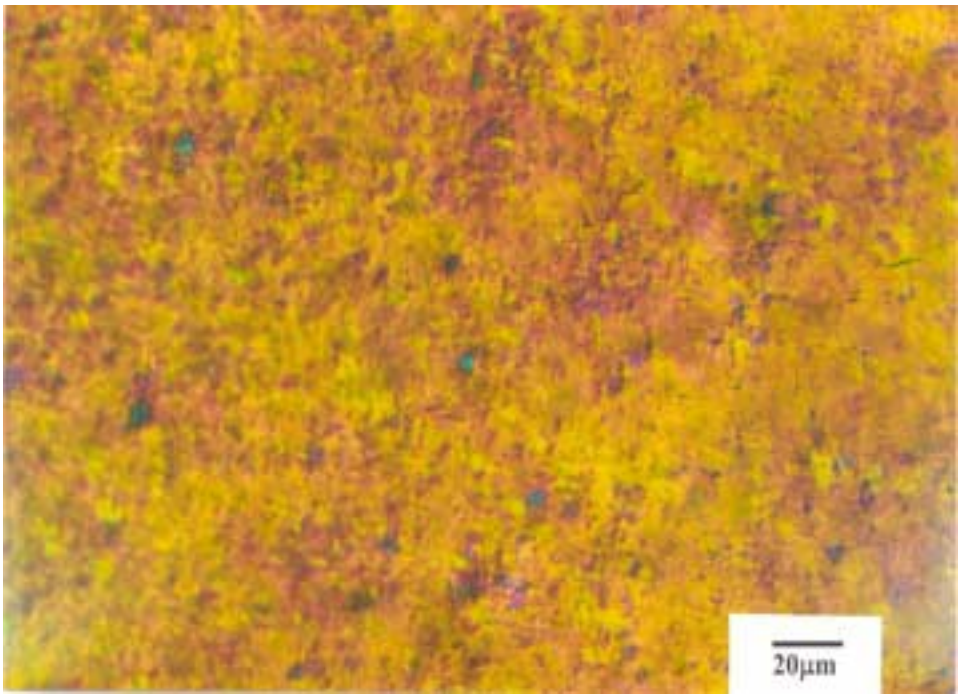

Figure 5.2 Optical micrograph of 1.0% cloisite 20A + PAI nanocomposite

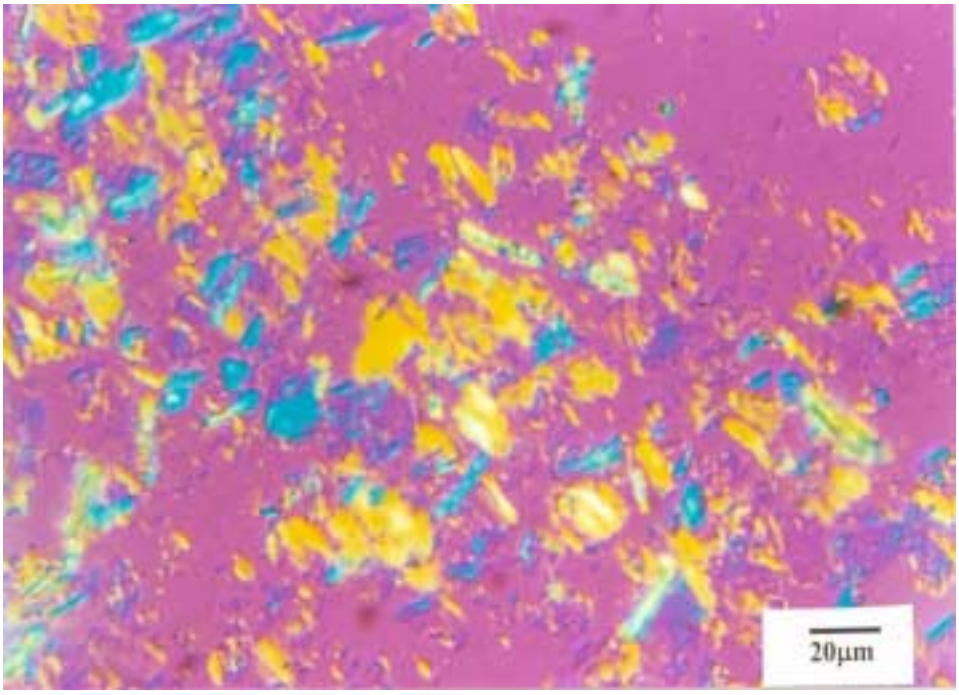

Figure 5.3 Optical micrograph of 3.0% cloisite Na^+ + PAI nanocomposite

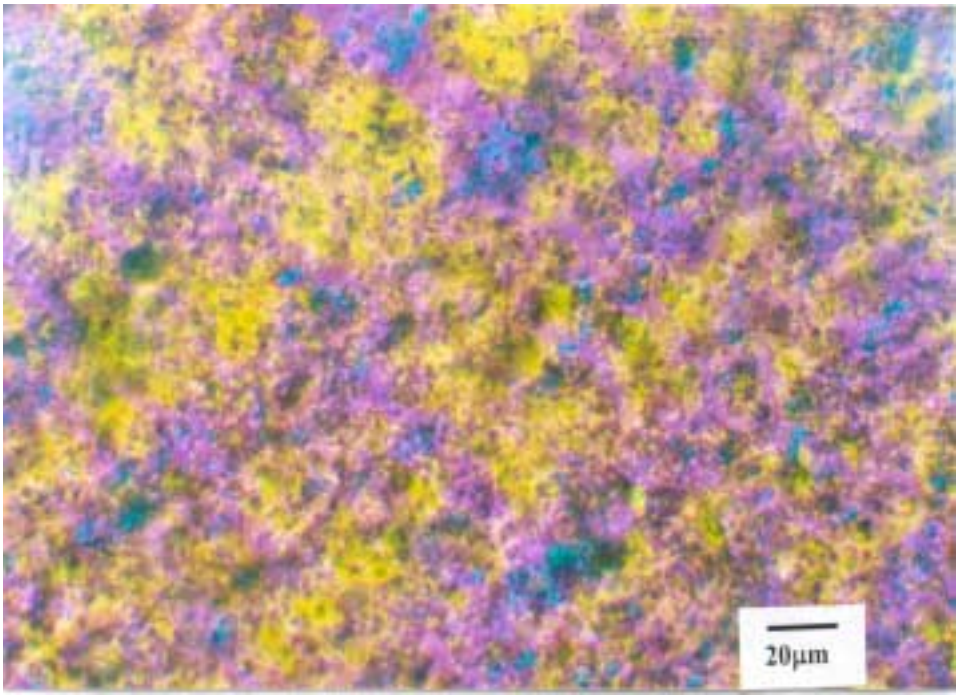

Figure 5.4 Optical micrograph of 3.0% cloisite20A + PAI nanocomposite

A polarizing optical microscope was used to study the dispersion of clay. As clearly seen in optical pictures, agglomerates of clay (blue colored) were found in case of cloisite Na^+ at both concentrations. In case of cloisite 20A, a uniform distribution of clay was observed at 1.0% and 3.0% clay concentrations. This behavior suggests the immiscibility of Na^+ hydrophilic clay with hydrophobic PAI polymer. However a good dispersion was observed in case of more organophilic clay 20A and organophilic PAI polymer. The optical results indicated the Na^+ clay as a bad partner for PAI system.

X-ray diffraction technique was also used to study the dispersion of clay in a PAI matrix. **Figure 5.5** shows the x-ray diffraction pattern of clay Na^+ + PAI composite and clay 20A + PAI composite.

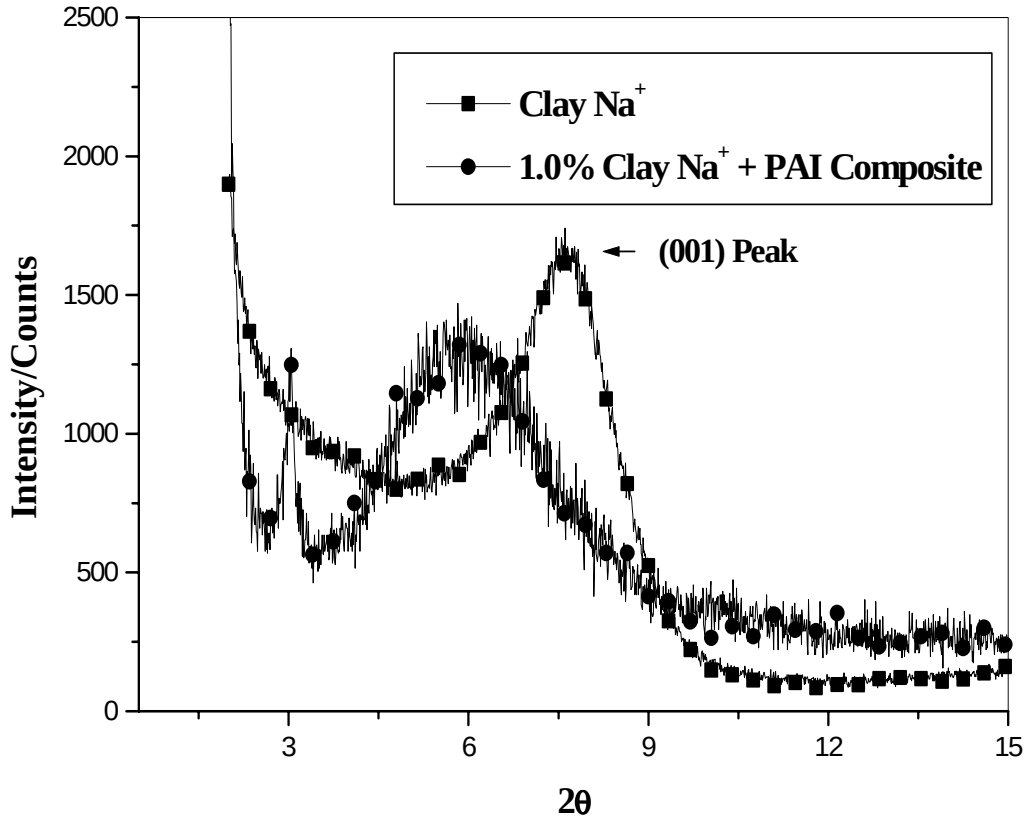

Figure 5.5 X-ray diffraction pattern of clay Na^+ and clay Na^+ + PAI composite

As seen in the diffraction pattern, no complete disruption of the (001) clay peak was observed in case of clay Na^+. Though there was a shift in (001) peak to the lower 2θ values, the order of clay platelets was very well retained even at low percentage. This suggests the tendency of clay to agglomerate inside the polymer matrix. This happens if the polymer and clay systems are immiscible[1,2,11-16,22-25,52].

Figure 5.6 is a x-ray diffraction pattern of clay 20A and clay 20A + PAI composite. At 1.0% clay, complete disruption of the (001) peak was observed. This suggests a uniform distribution of clay inside a polymer matrix.

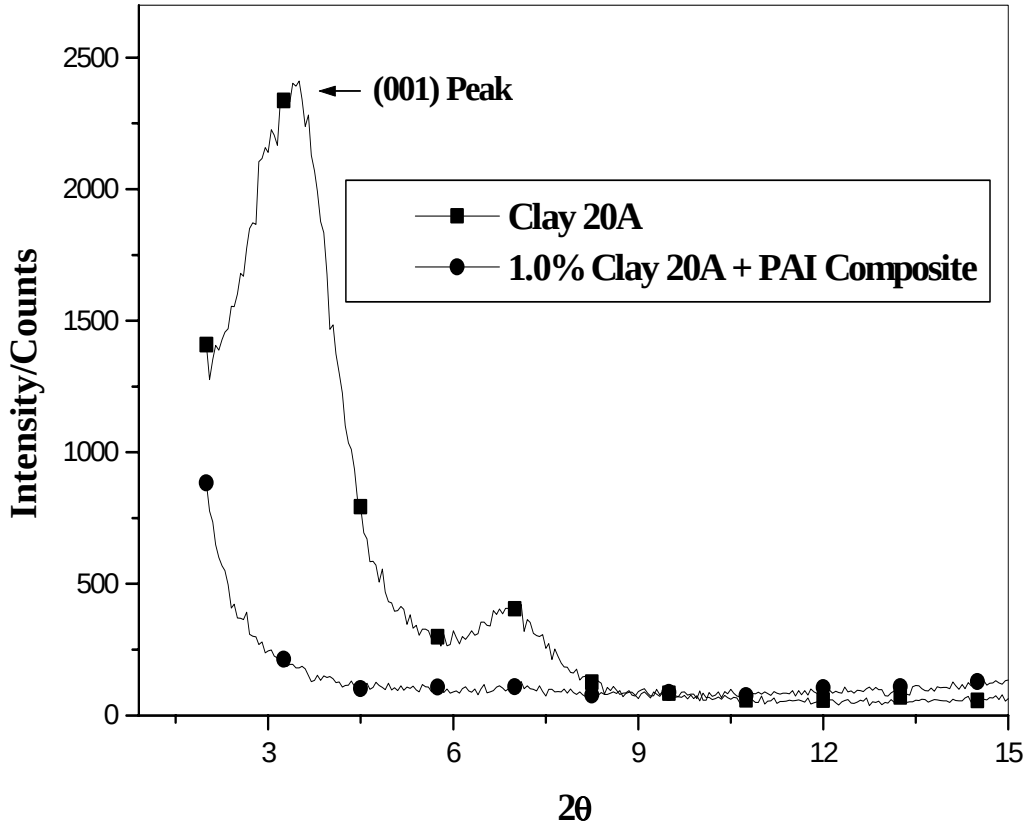

Figure 5.6 X-ray diffraction pattern of clay 20A and clay 20A + PAI composite

5.1.1 Conclusion based on Type of Clay

The optical microscopy and x-ray diffraction data suggested the miscibility problems of clay Na^+ with PAI system. Clay Na^+ is well suited for hydrophilic systems due to the absence of any organic surface modifier. On the other hand clay 20A which is more organophilic clay showed good dispersion in the PAI matrix indicating miscibility. From the data obtained with the help of optical microscopy and x-ray diffraction, clay 20A whose chemical name is cloisite 20A was chosen for the PAI system. In the thesis cloisite 20A is referred as **Montmorillonite (MMT)**.

5.2 Dispersion

Dispersion of MMT into PAI was studied by polarizing optical microscopy, x-ray diffraction technique, transmission electron microscopy and scanning electron microscopy.

5.2.1 Optical Microscopy

Distribution of clay platelets in PAI was studied by polarizing optical microscopy. It was used to study the miscibility as well as dispersion of clay into PAI from 1.0%-3.0% clay concentration. Polarizing optical microscopy helps to know whether platelet aggregation had taken place or not.

Figure 5.7 is an optical micrograph picture of 1.0% clay composite. The average clay size is 3.25μm and the picture shows uniform distribution of clay platelets in PAI matrix.

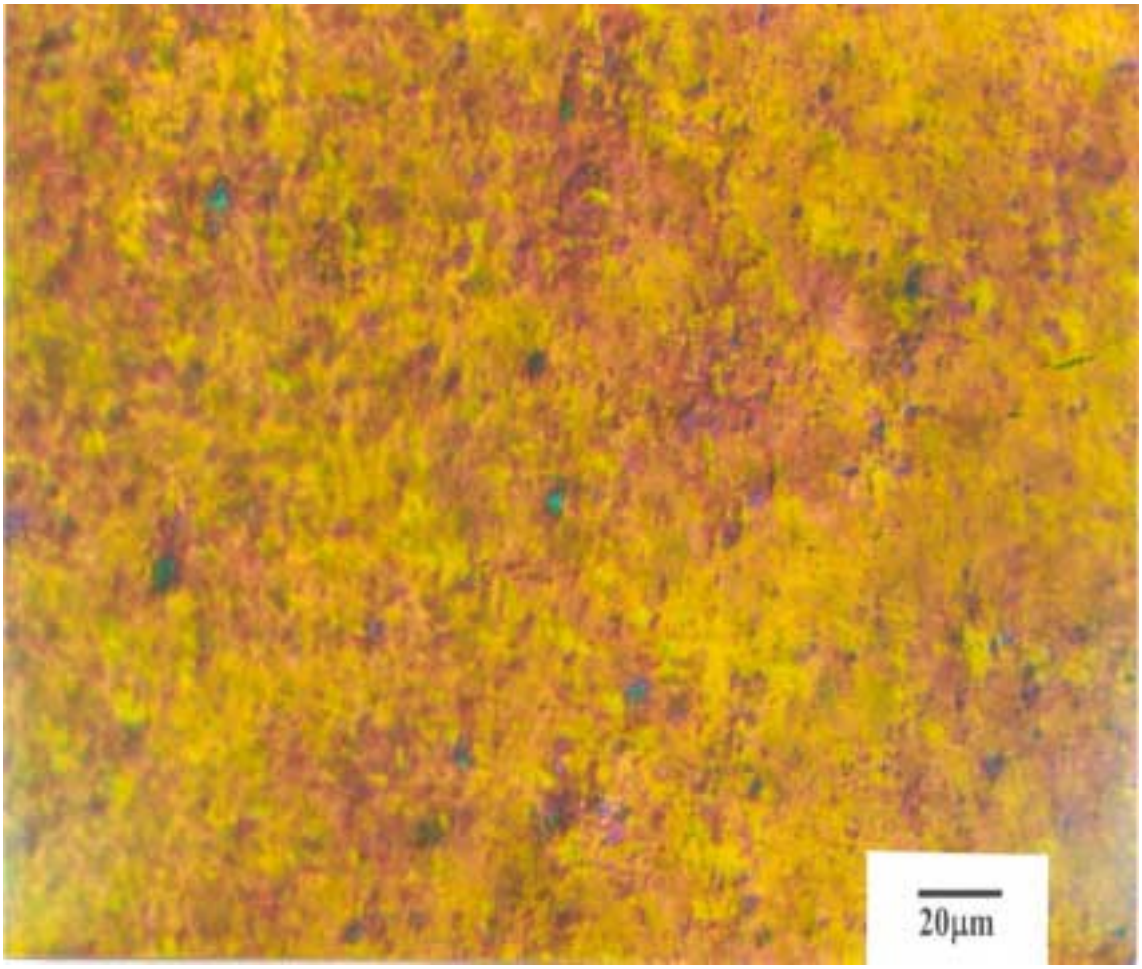

Figure 5.7 Optical micrograph of 1.0% clay composite

Figure 5.8 is an optical micrograph picture of 1.5% clay composite. The average clay size is 4.95μm. Increase in clay concentration has increased the size of clay platelets. Uniform distribution of clay platelets was observed for 1.5% clay composite.

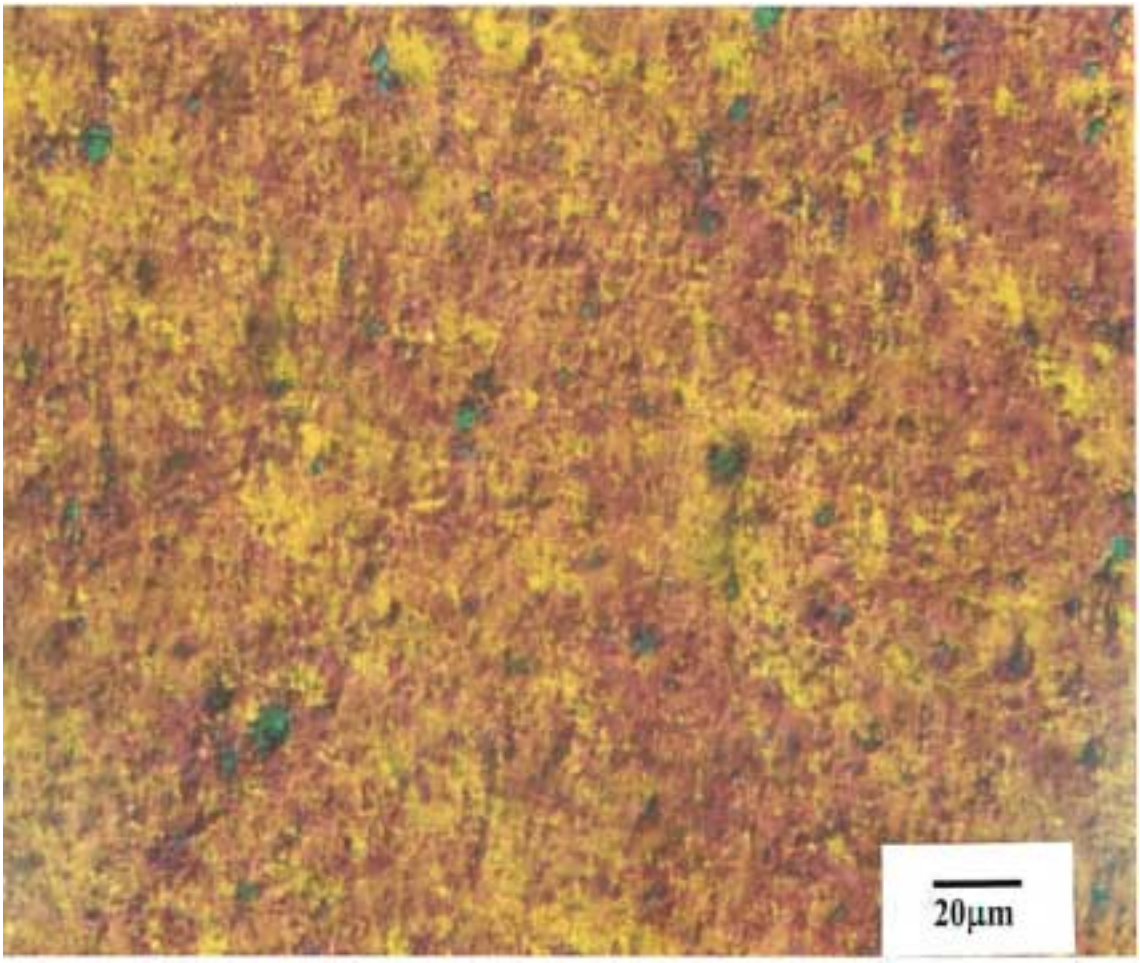

Figure 5.8 Optical micrograph of 1.5% clay composite

Figure 5.9 is an optical micrograph picture of 2.0% clay composite. The average clay platelet size is 5.69μm. Increase in clay concentration increased the size of clay platelets but no platelet agglomerates were observed showing good distribution of clay platelets.

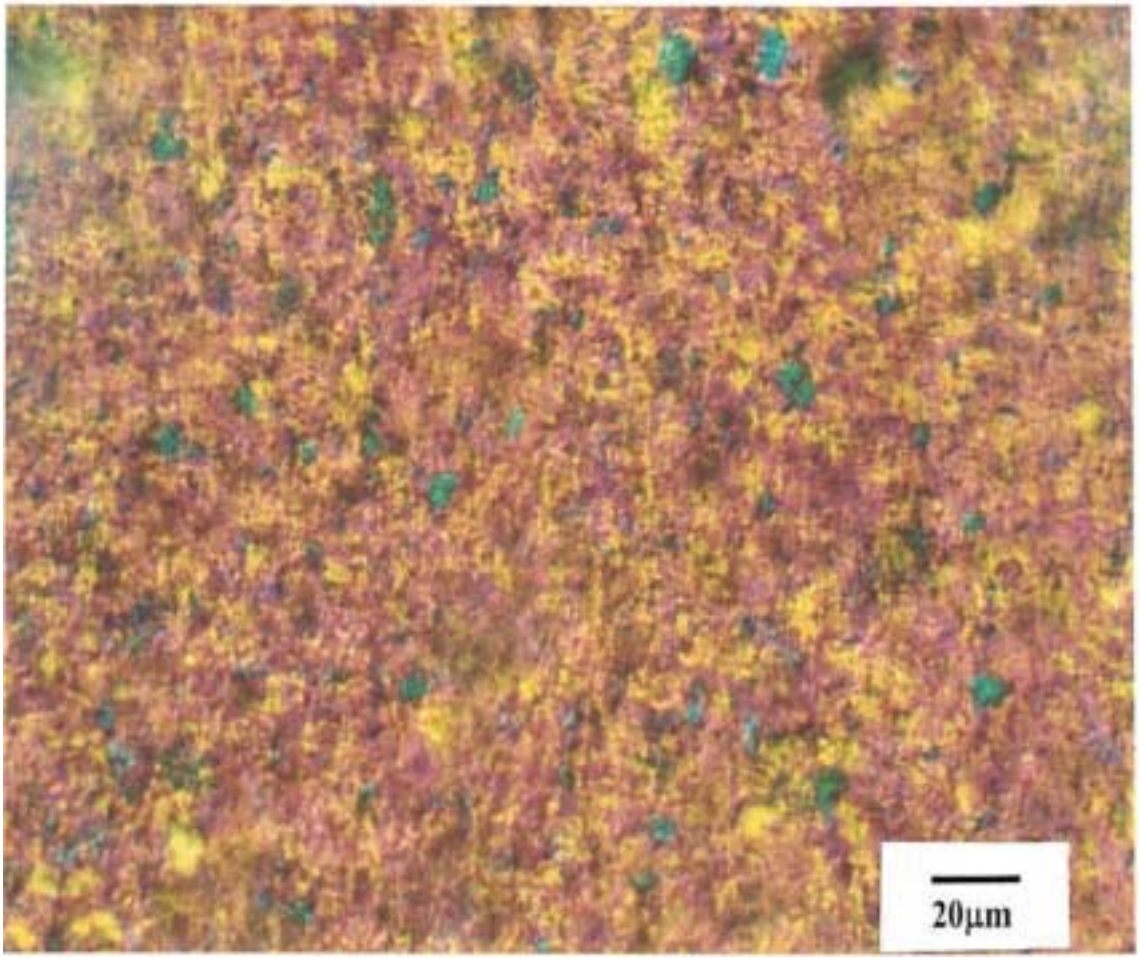

Figure 5.9 Optical micrograph of 2.0% clay composite

Figure 5.10 is an optical micrograph picture of 2.5% clay composite. 2.5% clay concentration showed initial signs of clay agglomeration. The agglomerates were small with average size of 7.43μm. These small agglomerates were found uniformly distributed over entire sample.

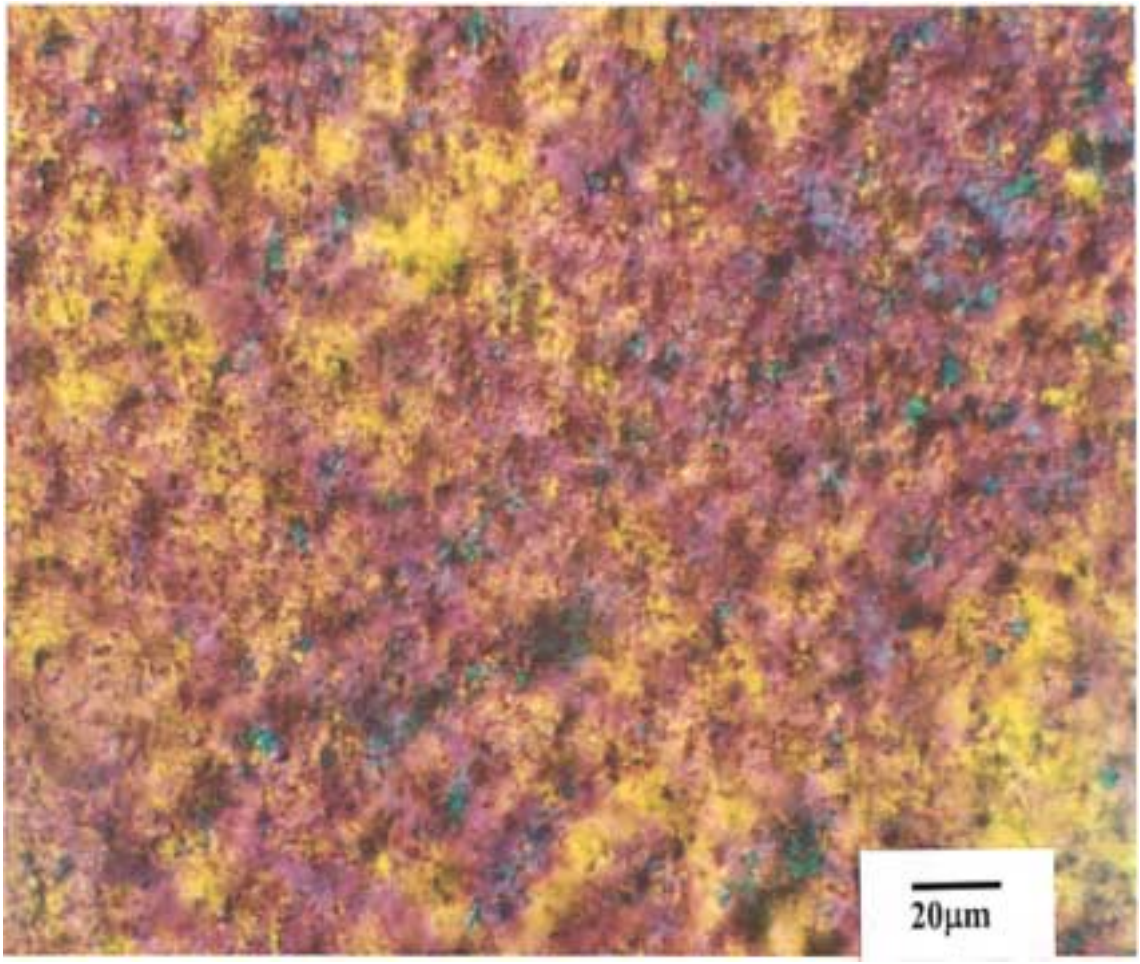

Figure 5.10 Optical micrograph of 2.5% clay composite

Figure 5.11 is an optical micrograph picture of 3.0% clay composite. 3.0% clay composite showed clear signs of clay agglomeration. Average size of agglomerates was 8.13μm. Interestingly these agglomerates were found distributed uniformly over entire sample.

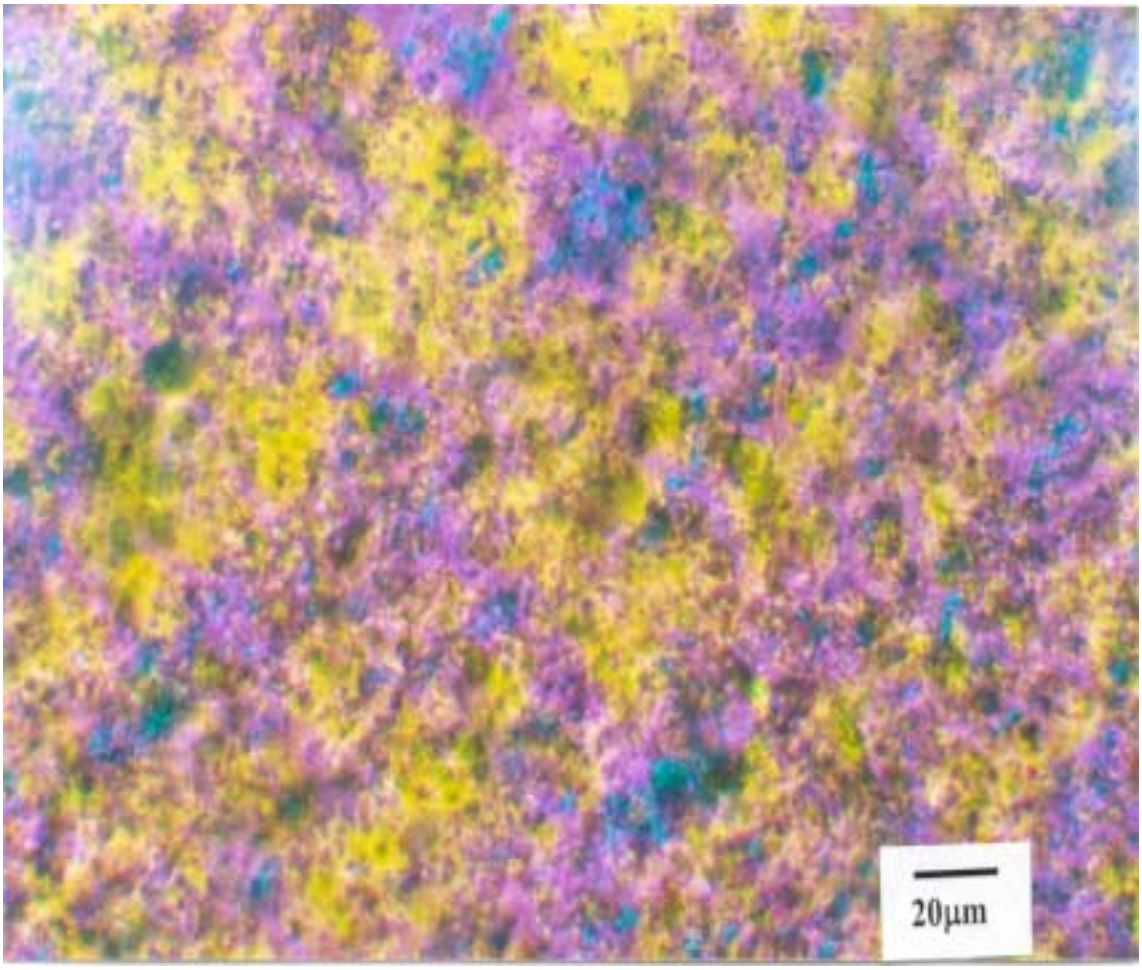

Figure 5.11 Optical micrograph of 3.0% clay composite

5.2.2 X-ray Diffraction (XRD)

XRD was used to characterize the crystallographic structure of montmorillonite. **Figure 5.12** is a x-ray diffraction pattern of a montmorillonite. Montmorillonite is a layered silicate with an interlayer spacing of $10A^{o}$[59]. As shown in figure, the organophilically treated montmorillonite have two characteristic peaks at low 2Θ equal to

7.098^{o} and 3.498^{o}. The peak 7.098^{o} corresponds to basal spacing of 12.54A^{o} and the peak 3.498^{o} corresponds to basal spacing of 25.24A^{o}.

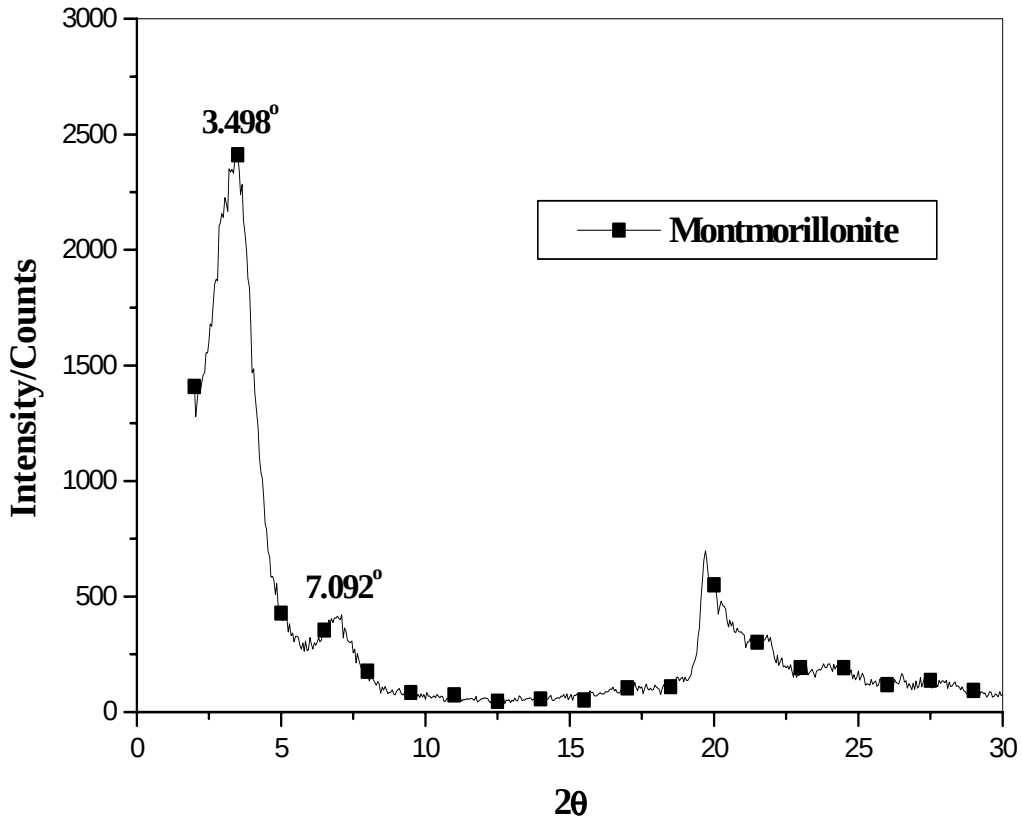

Figure 5.12 X-ray diffraction pattern of Montmorillonite

The peak at 2Θ equal to 3.498^{o} is a (001) peak[52,54]. Two states of dispersion are obtained when montmorillonite swells due to secondary component migration. When the basal spacing increases and the order is retained, an intercalated composite is obtained. Absence of diffraction peaks corresponding to the interlayer basal spacing is indicative of the disruption of ordered platelet separation leading to an exfoliated dispersion[1,3-7,11-16,52].

Figure 5.13 is a x-ray diffraction pattern of montmorillonite and blank polyamide-imide.

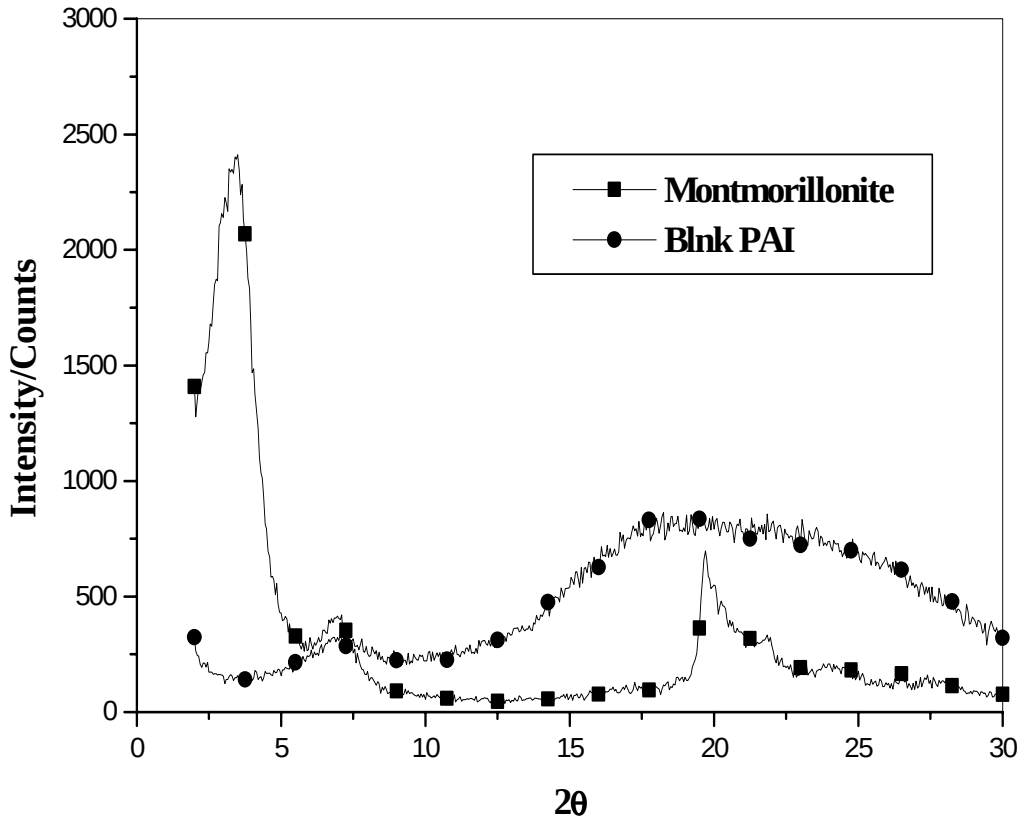

Figure 5.13 X-ray diffraction pattern of montmorillonite & polyamide-imide

PAI is an amorphous polymer, which is evident from the diffraction pattern. The polymer doesn't have any sharp peaks but has a big amorphous peak starting around 2Θ equal to 10^{o}. PAI has a small peak approximately at 2Θ equal to 8^{o}, which overlaps the clay peak at 2Θ =7.092^{o}.

Figure 5.14 is a x-ray diffraction pattern of montmorillonite, blank polyamide-imide and 1.0% clay composite.

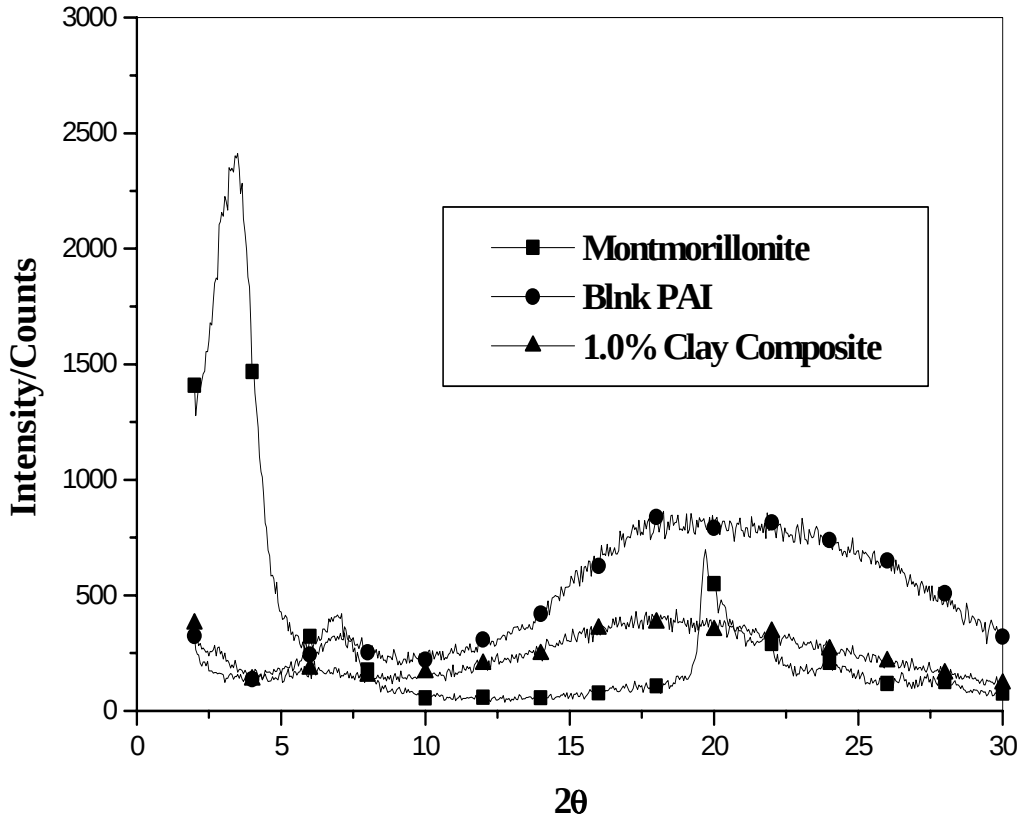

Figure 5.14 X-ray diffraction pattern of montmorillonite, blank PAI & 1.0% clay composite

As shown in **Figure 5.14**, PAI + montmorillonite composite containing 1.0% montmorillonite (based on solid weight content of PAI) shows no x-ray diffraction peak corresponding to the interlayer basal spacing. The disruption of the ordered montmorillonite is indicative of an exfoliated dispersion.

Figure 5.15 is a x-ray diffraction pattern of montmorillonite, 1.5%, and 2.0% clay composite.

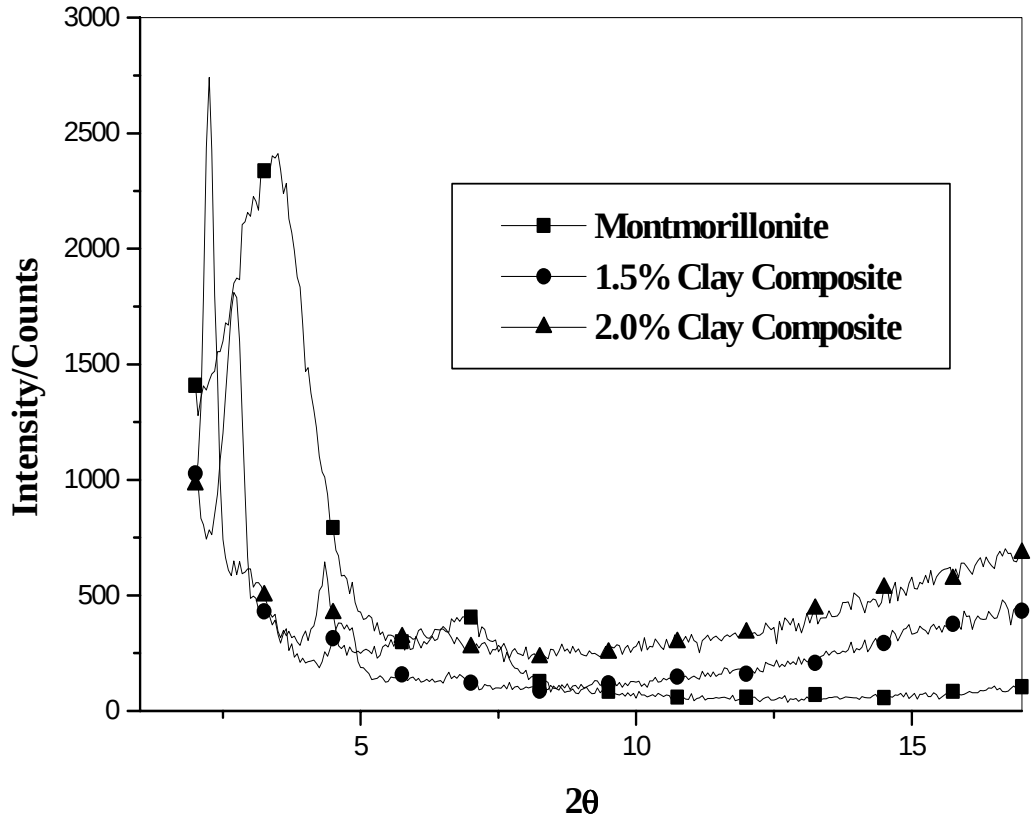

Figure 5.15 X-ray diffraction pattern of montmorillonite, 1.5% & 2.0% clay composite

As shown in **Figure 5.15** the shift in clay peak has observed for 1.5% & 2.0% (based on solid weight content of PAI) clay concentration. Intense reflections were observed for 1.5% and 2.0% composites. These intense reflections indicate the high structural regularity. This shows that almost all of the clay platelets are successfully intercalated into polymer chains. In case of 1.5% composite the 3.004^{o} clay peak has shifted to 2Θ equal to 2.701^{o} and 2.283^{o} for 2.0% composite respectively with a d spacing of 32.68A^{o} and 38.66A^{o} compared to clay d spacing of 25.24A^{o}. This

corresponds to an increase in interlayer spacing of 7.44A^{o} for 1.5% and 13.42A^{o} for 2.0% composite. Intercalated dispersion was observed in 1.5% and 2.0% clay composite. There was increase in basal spacing but the order was retained confirming intercalation.

Figure 5.16 shows the x-ray diffraction pattern of montmorillonite, 2.5% and 3.0% (based on solid weight content of PAI) clay composite.

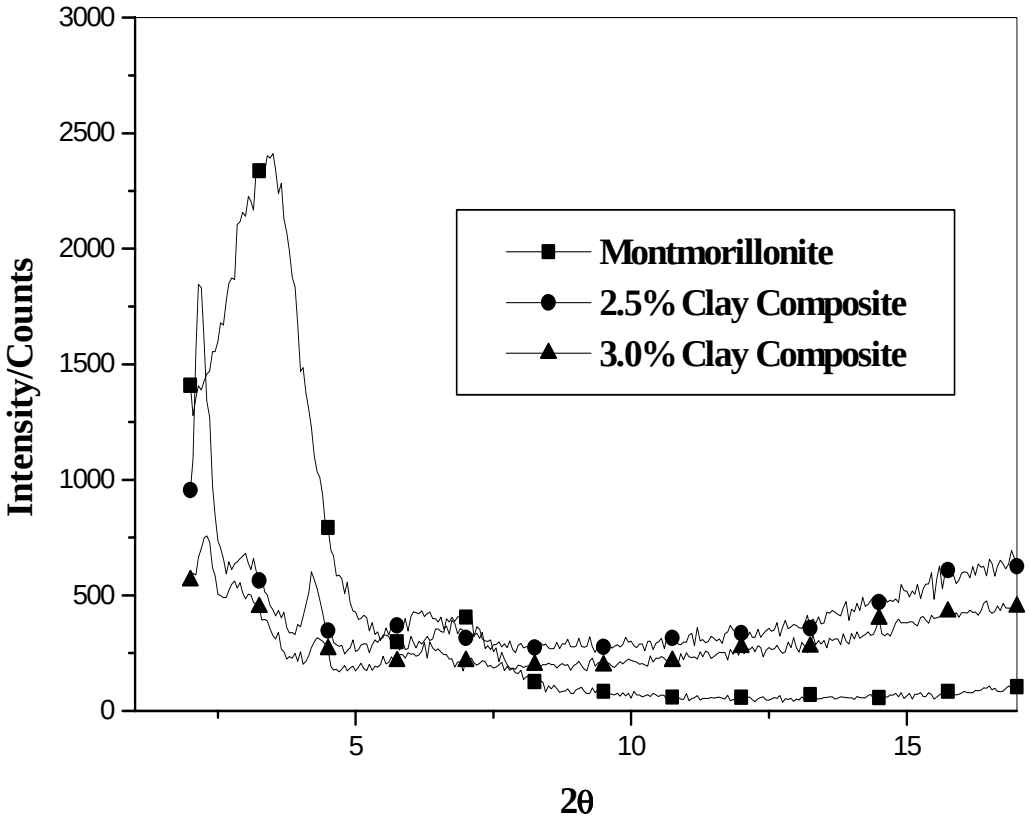

Figure 5.16 X-ray diffraction pattern of montmorillonite, 2.5% & 3.0% clay composite

As shown in **Figure 5.16** d spacing increases to 38.48A^{o} for 2.5% and 38.46A^{o} for 3.0% composite. The 3.004^{o} peak of clay has shifted to 2.294^{o} for 2.5% and 2.295^{o} for

3.0% composite. Complete disruption of clay platelets was not observed and though there was increase in d spacing compared to clay the order of clay platelets was retained showing a state of intercalated dispersion. No intense peak was observed for 3.0% nanocomposite indicating a loss of structural regularity. This shows that a small amount of clay is not getting intercalated at all. It is retaining its own identity i.e. neither intercalated nor exfoliated but forming immiscible or macro system.

5.2.3 Transmission Electron Microscopy (TEM)

Transmission electron micrograph of a 1.0% clay composite is shown in **Figure 5.17**. Individual crystallites of the silicate are visible as regions of alternating narrow, dark and light bands within the particle. **Figure 5.17**, which has a magnification of 288,000X with an average platelet separation of 28.12nm, is an indication of exfoliated dispersion.

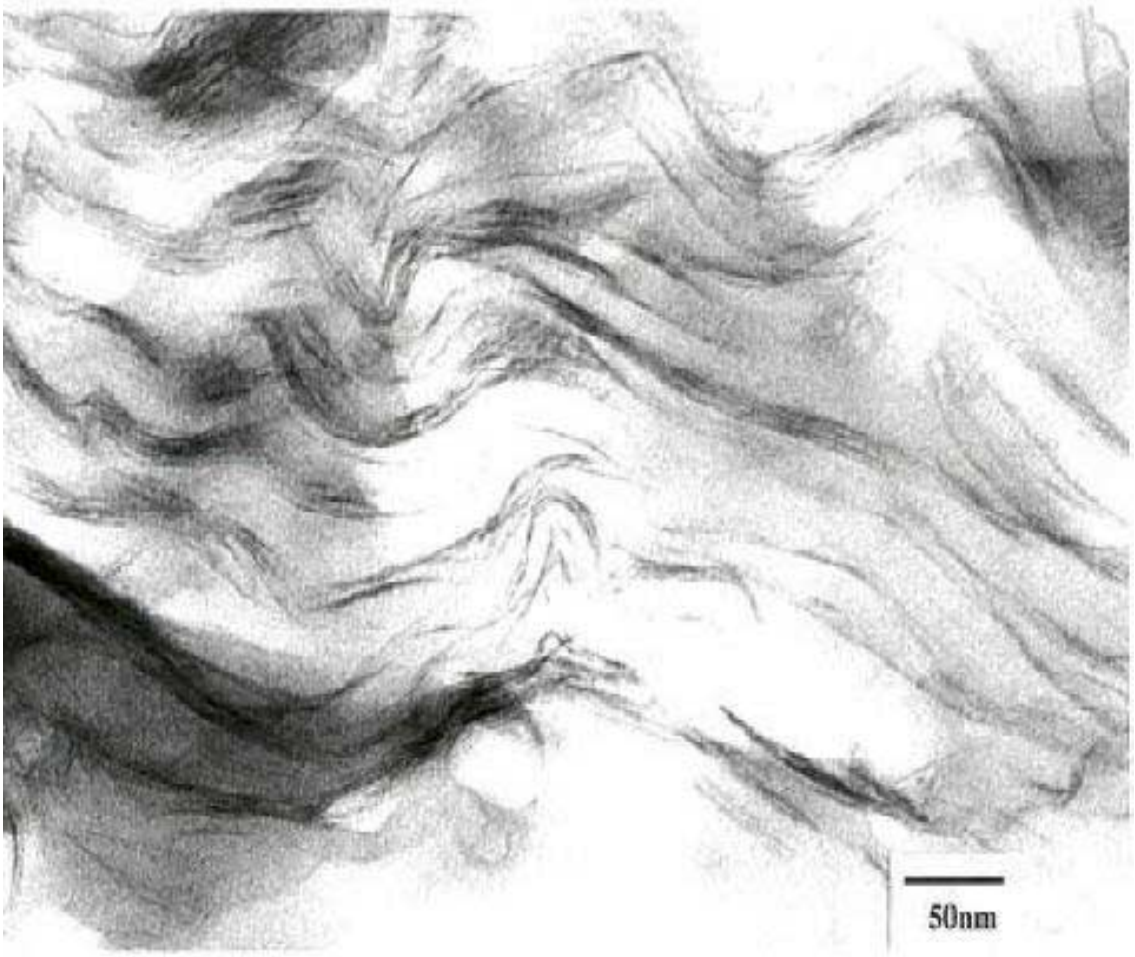

Figure 5.17 Transmission electron micrograph of 1.0% clay composite

The dark lines, which are the cross-sections of the thick silicate layers, have a variable thickness from $10A^{o}$ to $30A^{o}$.

Figure 5.18 is a Transmission electron micrograph of a 1.5% clay composite. The dark lines are the cross sections of thick silicate layers. The 1.5% clay composite shows the retention of ordered platelets with slight expansion of the gallery height to accommodate polymer, which is an indication of intercalated dispersion. The average platelet separation is 9.52nm. **Figure 5.18** has a magnification of 126,000X.

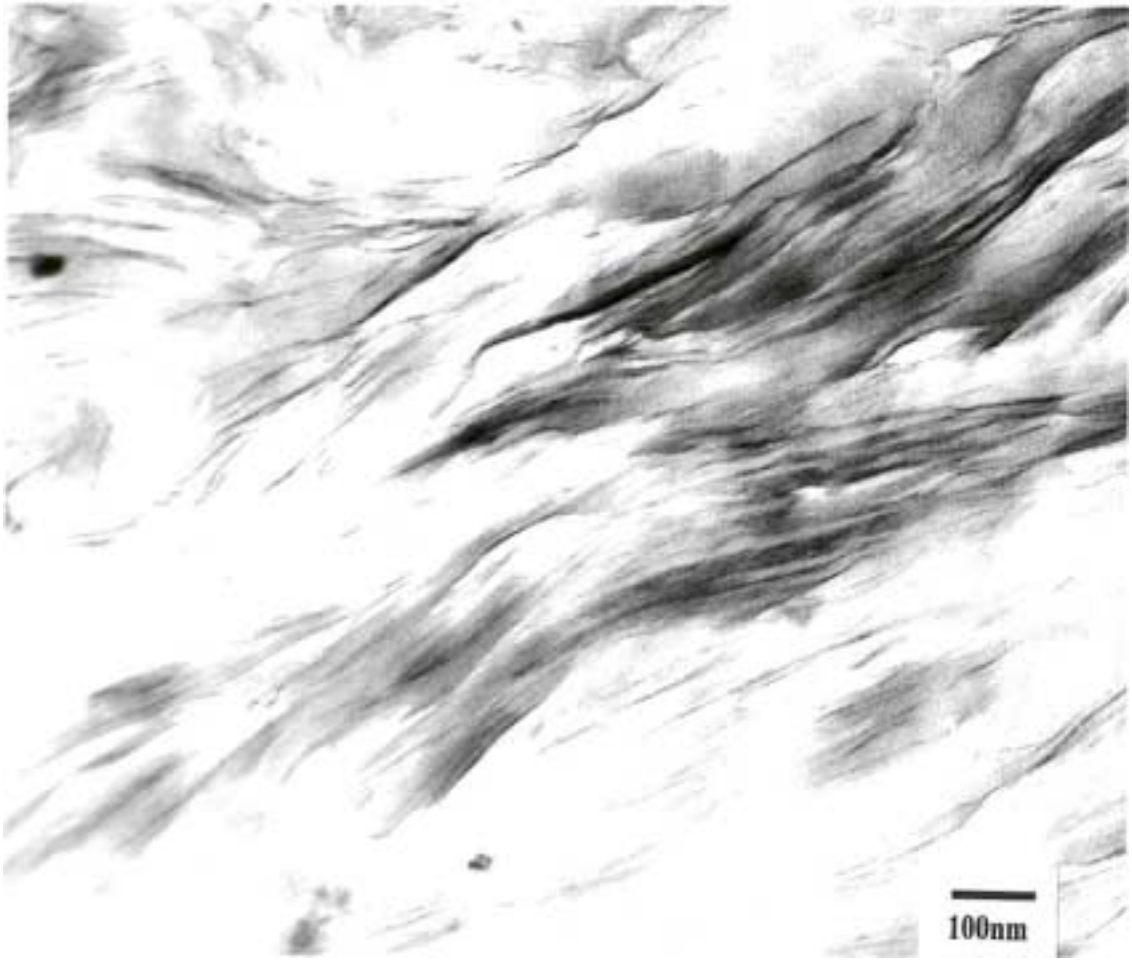

Figure 5.18 Transmission electron micrograph of 1.5% clay composite

Figure 5.19 is a Transmission electron micrograph of 2.0% clay composite, which is also showing an intercalated dispersion. The picture shows the average platelet separation of 12.71nm. The basal spacing has increased with retention of clay structures. The micrograph has a magnification of 70,000X.

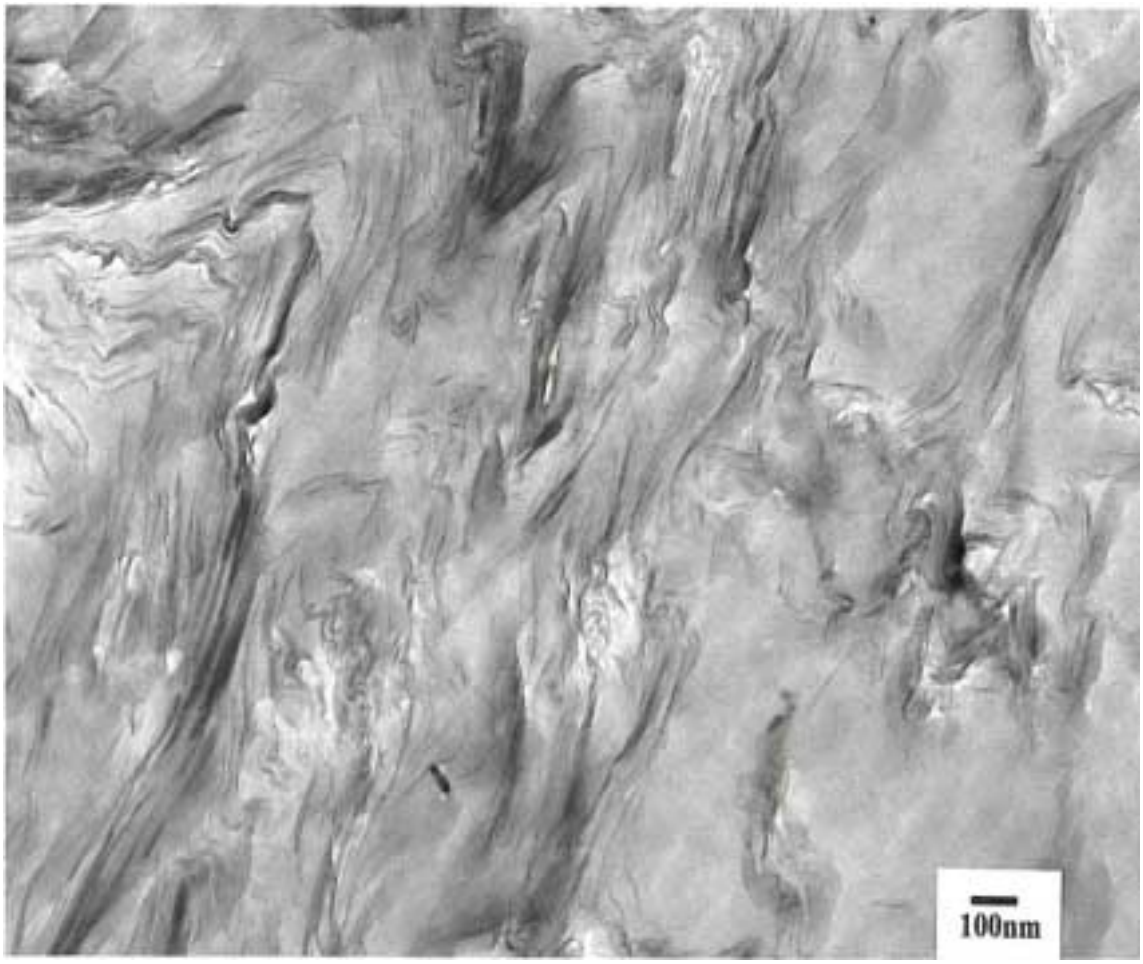

Figure 5.19 Transmission electron micrograph of 2.0% clay composite

An intercalated dispersion of 2.5% clay composite was observed and is shown in **Figure 5.20**. The average platelet separation from **Figure 5.20** was found as 11.28nm. The micrograph has a magnification of 70,000X.

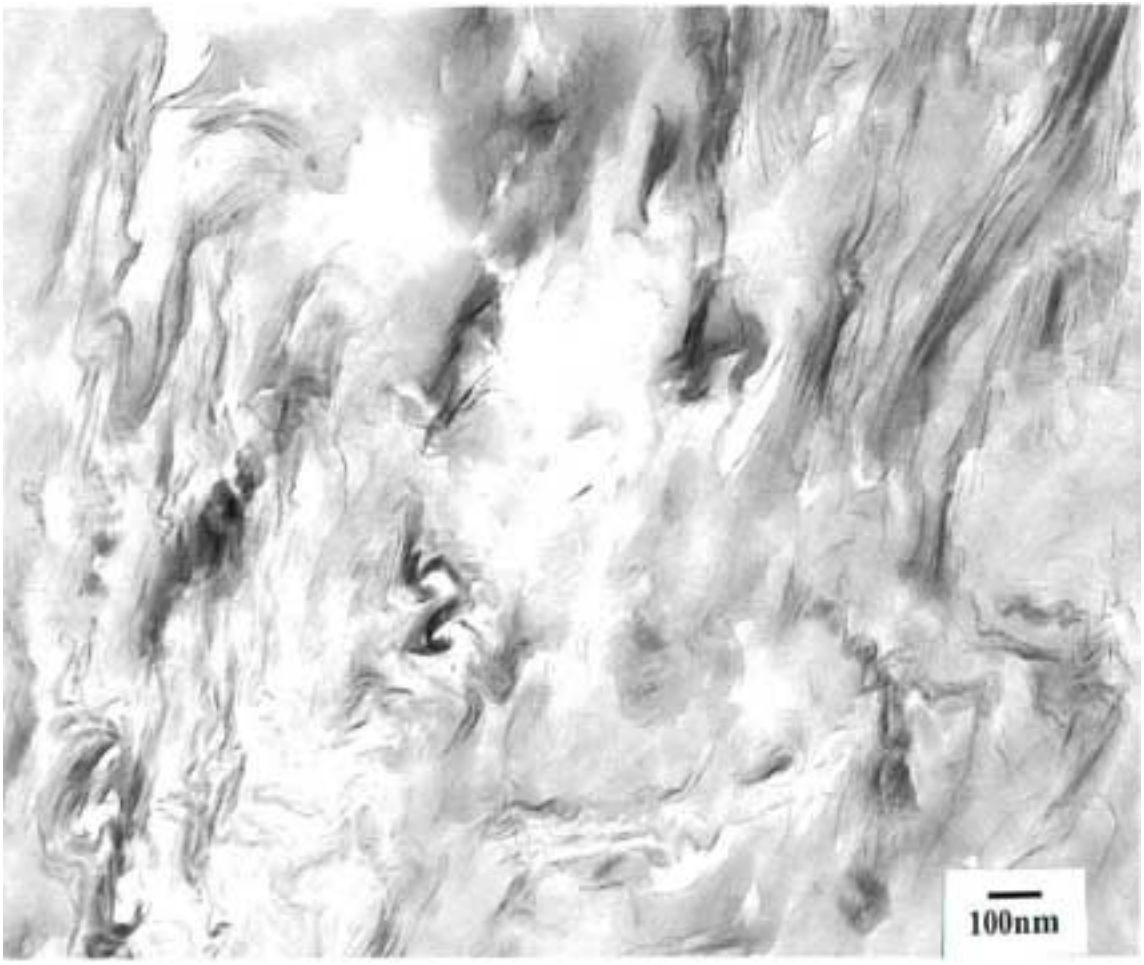

Figure 5.20 Transmission electron micrograph of 2.5% clay composite

Figure 5.21 is Transmission electron micrograph of 3.0% clay composite. 3.0% micrograph showed the average platelet separation of 8.28nm. The micrograph has a magnification of 70,000X.

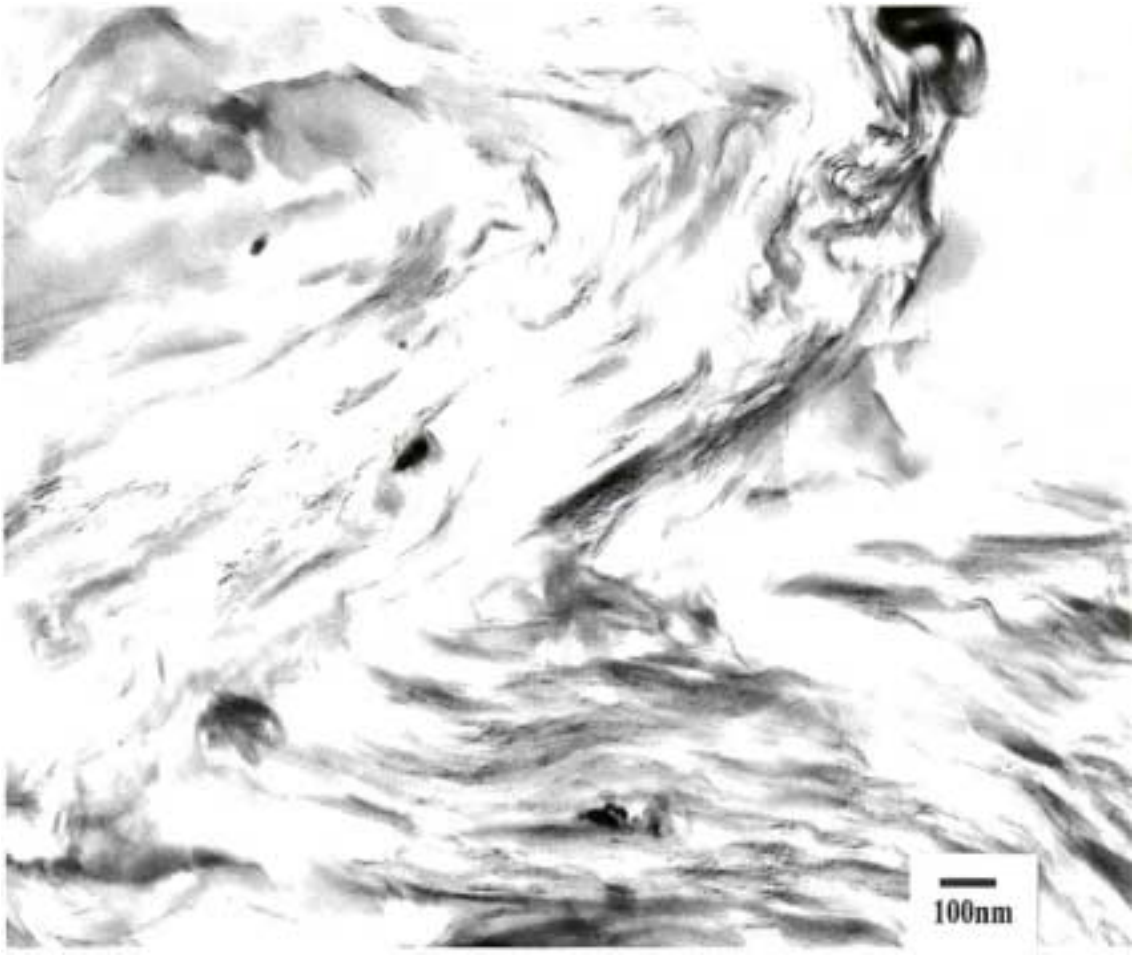

Figure 5.21 Transmission electron micrograph of 3.0% clay composite

5.2.4 Scanning Electron Microscopy (SEM)

The morphology of pure montmorillonite and montmorillonite + PAI is illustrated in **Figure 5.22-5.28**. Electron micrographs with magnification varying from 150X to

2000X were taken from cast film surfaces. The surface of the film was polished in order to see the dispersion of clay.

Figure 5.22 and 5.23 show the typical microstructure of montmorillonite. As we see in the picture, montmorillonite is composed of small platelets stacked one above the other. Montmorillonite has dense platelet morphology.

The scanning electron micrographs of 1.0%, 1.5%, 2.0%, 2.5% and 3.0% clay composites are shown in **Figure 5.24-5.28.** Scanning electron microscopy showed significant morphological similarities between pure montmorillonite and montmorillonite + PAI. As seen in the pictures, the basic shape of montmorillonite was retained. The micrographs showed the even dispersion of clay throughout the polymer matrix and also there was no sign of clay agglomeration. The average size of a clay platelet in composite was found very close to the average size of a clay platelet in pure montmorillonite. This also supports the fact that there was no degradation of clay platelets in a composite[28,36,53].

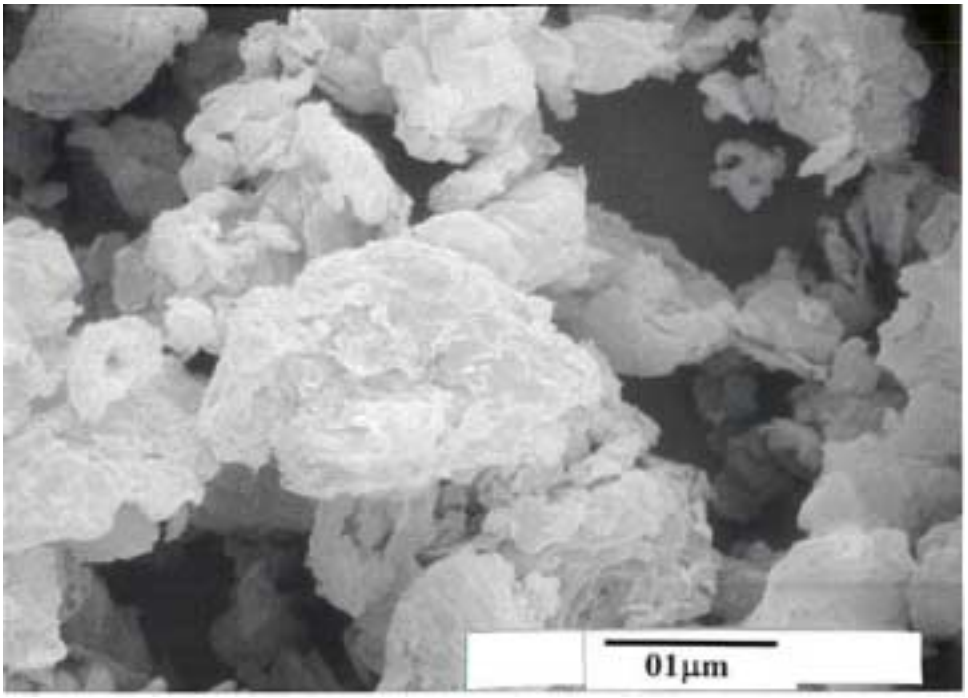

Figure 5.22 Scanning electron micrograph of montmorillonite

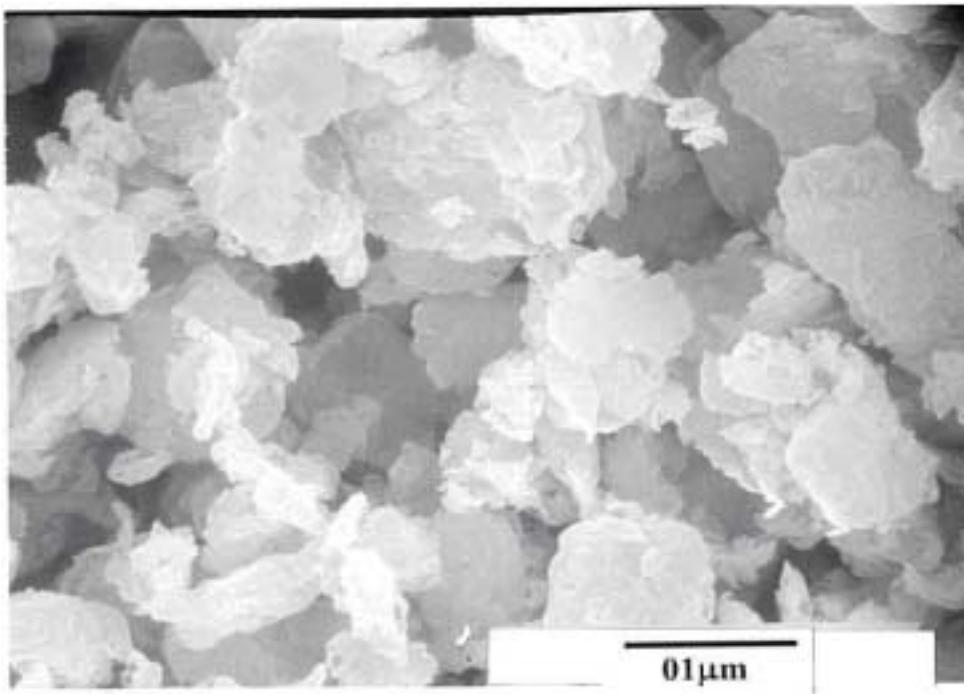

Figure 5.23 Scanning electron micrograph of montmorillonite

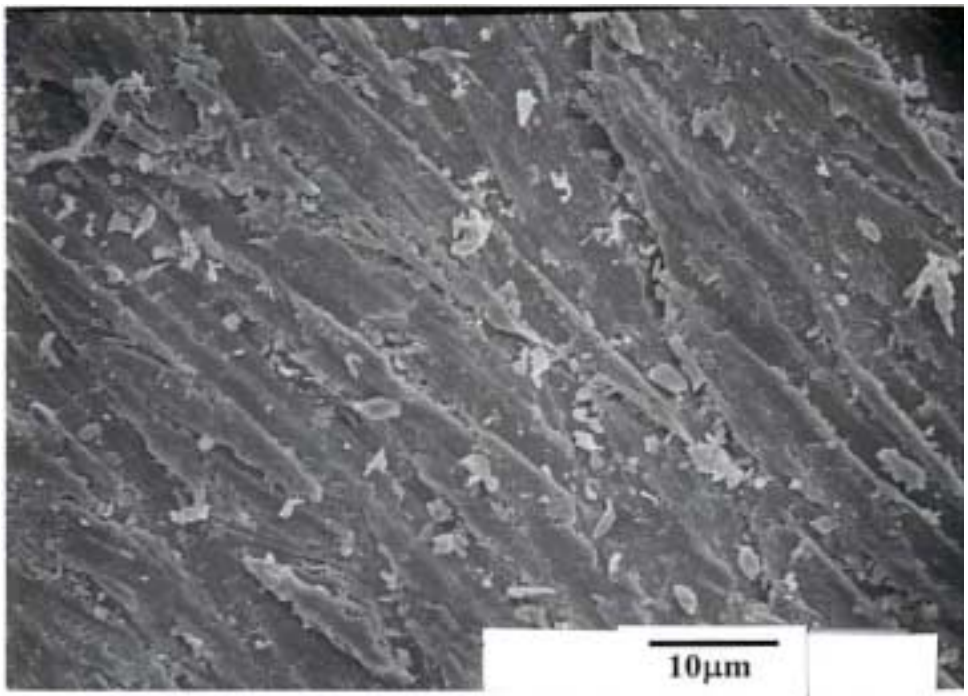

Figure 5.24 Scanning electron micrograph of 1.0% clay composite

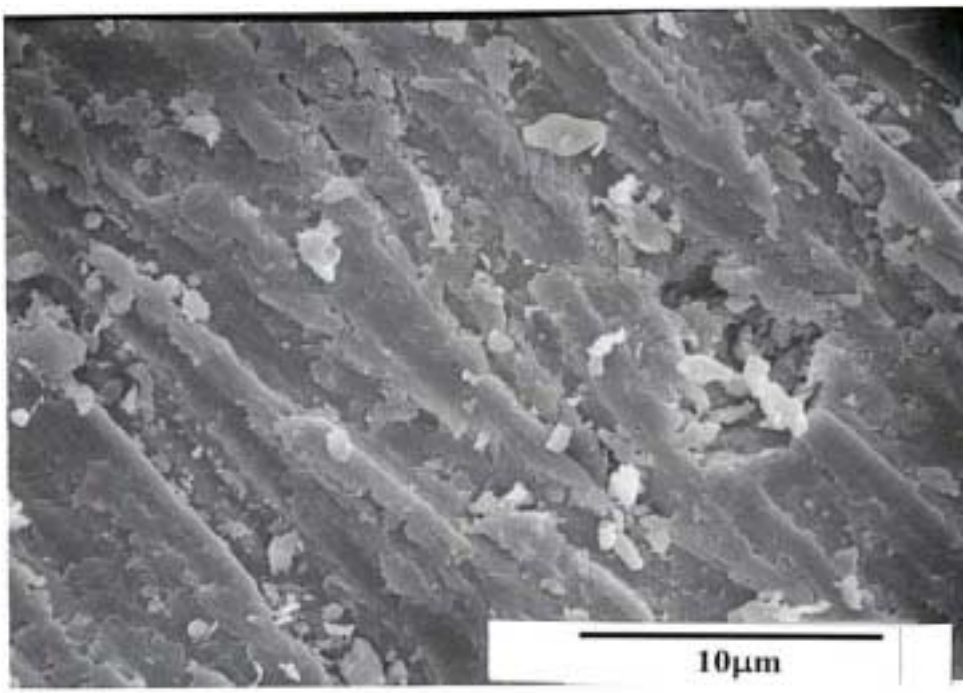

Figure 5.25 Scanning electron micrograph of 1.5% clay composite

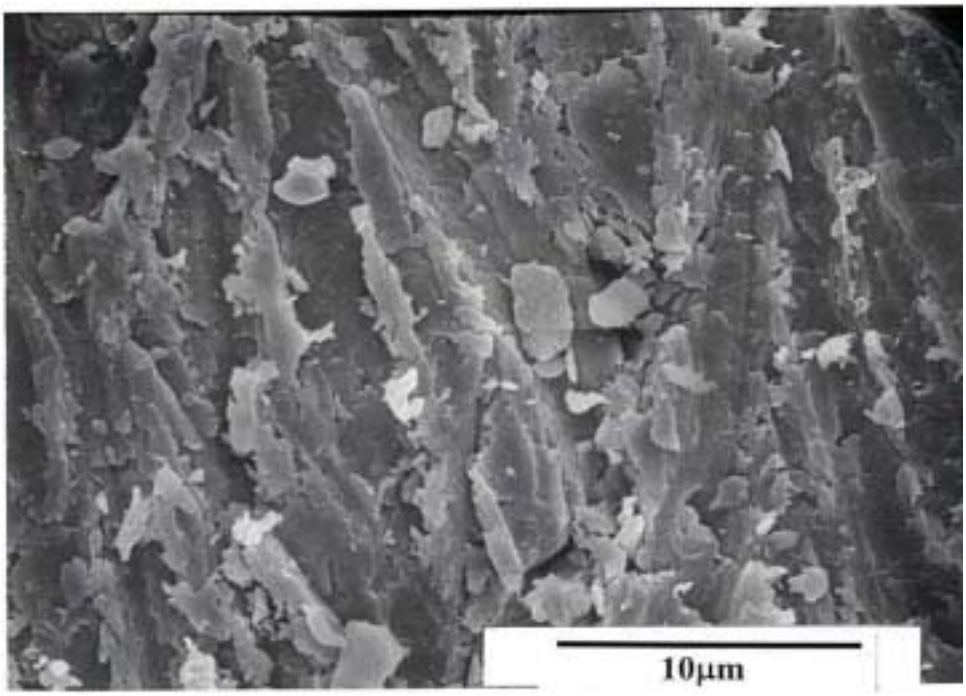

Figure 5.26 Scanning electron micrograph of 2.0% clay composite

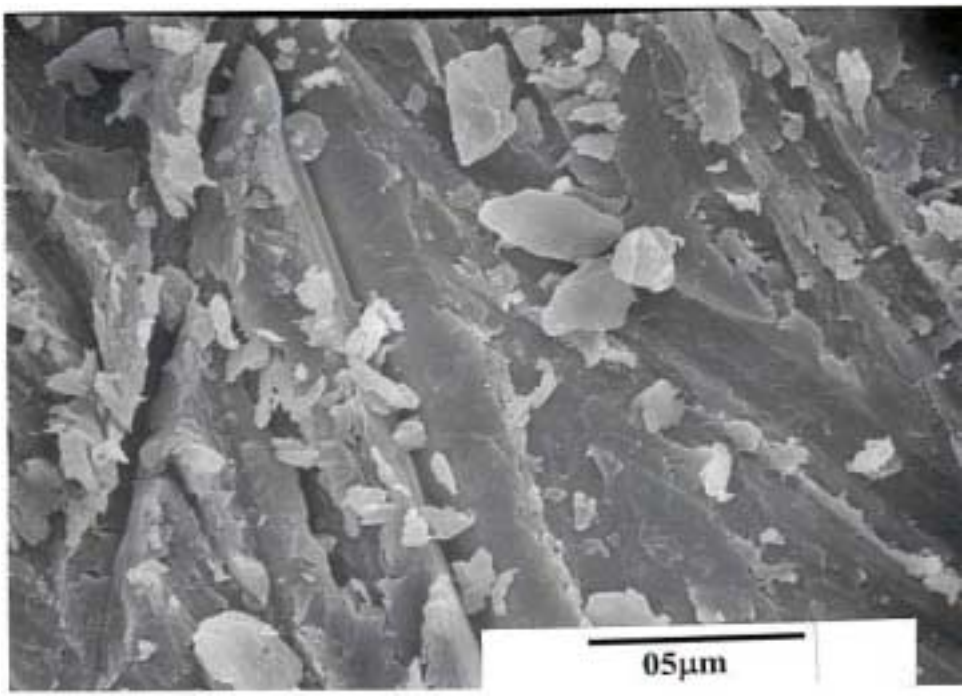

Figure 5.27 Scanning electron micrograph of 2.5% clay composite

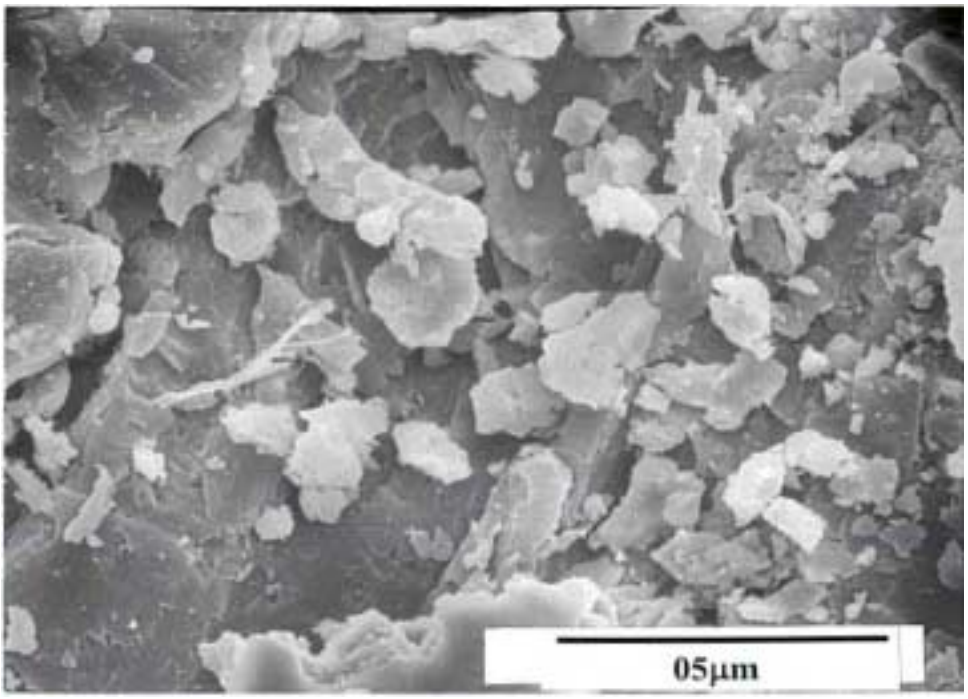

Figure 5.28 Scanning electron micrograph of 3.0% clay composite

5.2.5 Conclusions Based on Dispersion of MMT in PAI

1. Optical microscopy showed uniform distribution of clay platelets into PAI. Initial signs of agglomeration were observed at 2.0% clay concentration. 3.0% clay concentration showed significant increase in agglomeration with agglomerates uniformly distributed over entire sample.
2. XRD showed concentration dependent dispersion in the PAI nanocomposite system. Exfoliated dispersion was observed at (1.0%) low clay concentration. Increase in clay concentration from 1.5-3.0% showed intercalated dispersion. At low clay concentration, polymer clay interactions overcame the Van der Waals forces between silicate galleries and resulted in a complete disruption of clay structure. Increase in clay concentration, Van der Waals interaction started dominating polymer clay

interactions and resulted in a finite expansion of silicate galleries and retention of clay structure.

3. TEM confirmed XRD results. Wider platelet separation was observed for exfoliated (1.0%) dispersion. 1.5-3.0% clay composite showed platelet separation from 8-12nm indicating intercalated dispersion.
4. In general the SEM showed the even dispersion of clay platelets and absence of clay clumps in a composite supporting the results of the optical microscopy study.

5.3 Glass Transition

PAI is an amorphous polymer with T_g above 270^oC. A very high T_g is one of the reasons for high mechanical strength in PAI. Thus T_g is an important parameter, which dictates the end use property of the polymer. DSC was used to study the effect of MMT on the T_g of PAI.

5.3.1 Differential Scanning Calorimetry (DSC)

Figure 5.29 shows the effect of clay concentration on the T_g of PAI.

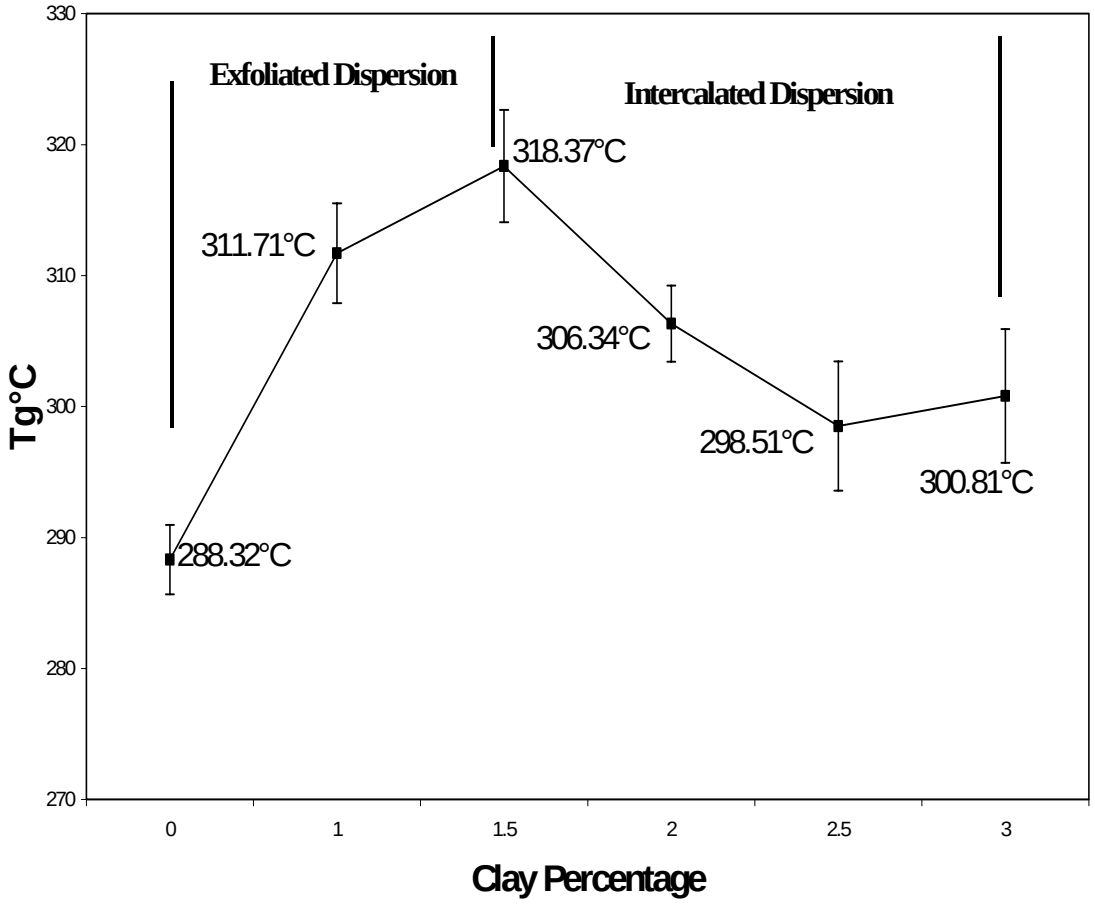

Figure 5.29 Effect of montmorillonite on glass transition temperature (T_g) of PAI nanocomposite

The introduction of 1.0% montmorillonite by weight into the PAI serves to substantially increase the T_g by 8.11%. Results on the intercalated dispersion are however mixed. At 1.5% by weight montmorillonite concentration an even higher T_g over that of the PAI is evident. However increasing the montmorillonite concentration serves to decrease the T_g by 6.25%, 3.43% and 5.75% for the 2.0%, 2.5% and 3.0% PAI nanocomposite. This result is analyzed in the context of the role of chain confinement

between the platelets in the intercalated systems presented by McKenna[27]. He observed that changes in the glass transition temperature due to constraint introduced by finite pore geometries were related to pressure effects of constraint during polymerization.

To explain what really happened at the molecular level, we have developed a model, which will help to understand the effect of MMT on T_g of PAI nanocomposites. **Figure 5.30** shows the exfoliated behavior observed at 1.0% MMT concentration.

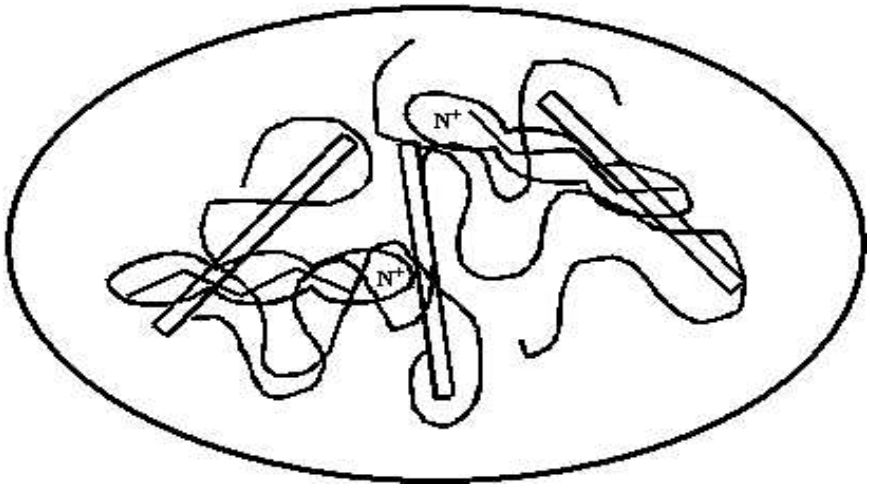

Figure 5.30 Exfoliated dispersion at 1.0% MMT concentration.

Glass transition temperature is a temperature, which corresponds to segmental motions of polymer chains on the molecular level. This is a localized phenomenon. Addition of stiff clay platelets acts as a reinforcement to polymer chains at molecular level. The presence of these stiff clay platelets obstructs the localized motions of polymer chains. This results in an increase in T_g from around 288^{o}C to around 311^{o}C.

Further addition of clay has increased T_g for 1.5% MMT concentration but from 2.0 – 3.0% MMT concentration lowering of T_g was observed. **Figure 5.31 and Figure 5.32** explains this behavior at molecular level.

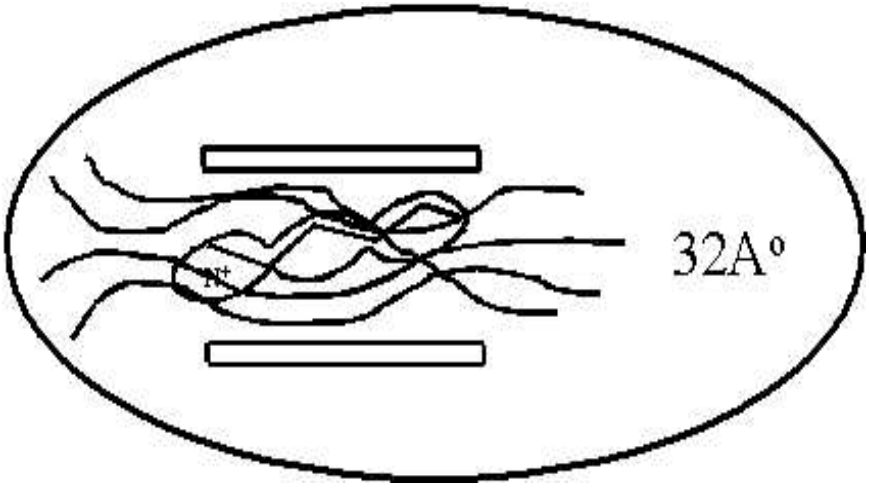

Figure 5.31 Intercalated dispersion at 1.5% MMT concentration. Increase in basal spacing from 25A° to 32A° was observed.

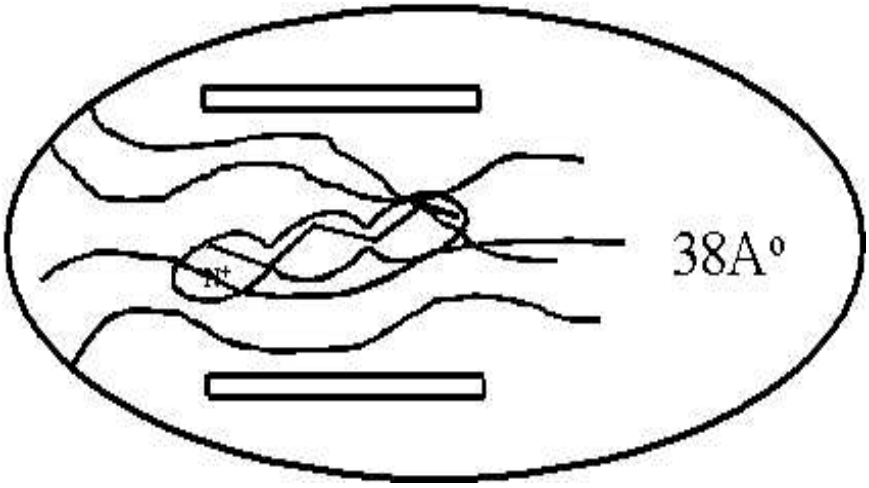

Figure 5.32 Intercalated dispersion at 2.0, 2.5 & 3.0% MMT concentration. Increase in basal spacing from 25A° to 38A° was observed.

MMT has a basal spacing equal to 25A°. As discussed in literature review, intercalation represents finite penetration of polymer chains into silicate galleries

resulting in expansion of galleries with retention of clay structure. Intercalated dispersion at 1.5% showed increase in basal spacing of $7A^{o}$ while 2.0, 2.5 and 3.0% showed increase of $13A^{o}$ over pure MMT.

Thus when there is more constraint (1.5%) on PAI chains, the mobility is reduced leading to an increase in T_g. When the constraint is approximately constant (between 2.0 & 3.0% MMT) the chain has an almost similar level of mobility leading to a relatively smaller change in T_g over base resin. Summarizing, addition of MMT has increased the T_g of PAI but it was observed that T_g is dispersion dependent phenomena where constraint (pressure) determines the T_g of polymer nanocomposites.

5.3.2 Conclusions Based on DSC

MMT affected the glass transition temperature (T_g) of PAI. T_g was not only found to be dependent on dispersion but also on the degree of dispersion. More chain confinement produces more pressure on polymer chains. More pressure on polymer chains results in increase in T_g. When confinement effect (pressure) is constant, similar T_g was observed from 2.0-3.0% clay composite.

5.4 Degradation studies

DSC results showed increase in T_g due to addition of clay. Results found to be dependent on dispersion rather than concentration of MMT. Due to very high T_g and retention of properties even after thermal aging, PAI is used in rockets and missiles. The thermal stability of PAI is an important parameter. MMT has alkyl ammonium cations between its galleries, which degrade at approximately $260^{o}C$. Therefore the influence of

MMT on PAI was investigated to determine the effect of the alkyl ammonium cations on a thermal degradation of nanocomposite.

5.4.1 Thermogravimetric Analysis

The effect of MMT on the thermal stability of PAI in air was studied by Thermogravimetric analysis technique. The experimental results are summarized in **Figure 5.33**.

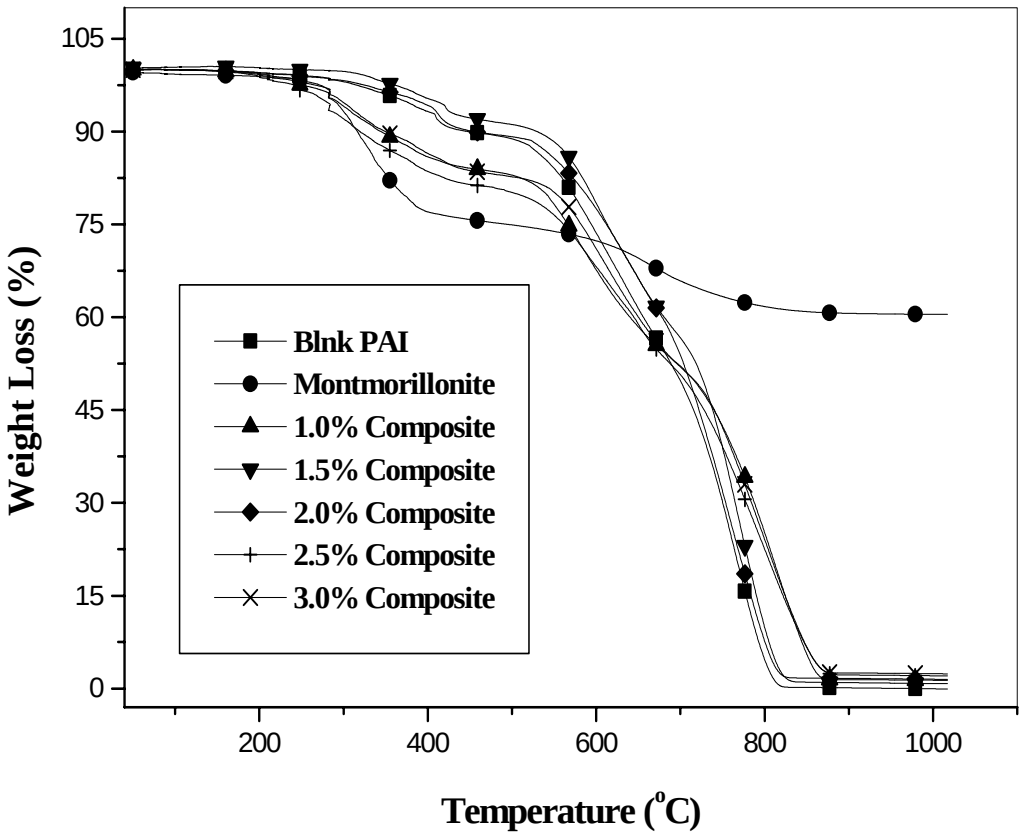

Figure 5.33 Thermogravimetric analysis curves for montmorillonite, blank PAI and PAI nanocomposites

Included in **Figure 5.33** are the TGA curves for the pristine montmorillonite, blank PAI, 1.0%, 1.5%, 2.0%, 2.5% and 3.0% clay composites. The analysis was carried out in an atmosphere of air. The experiments were carried out from 50^{o}C to 1000^{o}C at the heating rate of 20^{o}C per minute. As seen in the figure, montmorillonite shows two weight drops. The first weight drop is at around 265^{o}C with a weight loss of around 20% by weight. This initial weight loss in montmorillonite is due to the decomposition of quaternary alkyl ammonium cations situated between the layers of the clay platelets. The montmorillonite shows one more weight drop of 10% by weight at around 610^{o}C. No further weight drop was observed till 1000^{o}C, which shows the thermal stability of ceramics to high temperatures.

A graph of onset temperature, vs, individual systems was plotted to understand the relation of onset temperature with concentration of MMT.

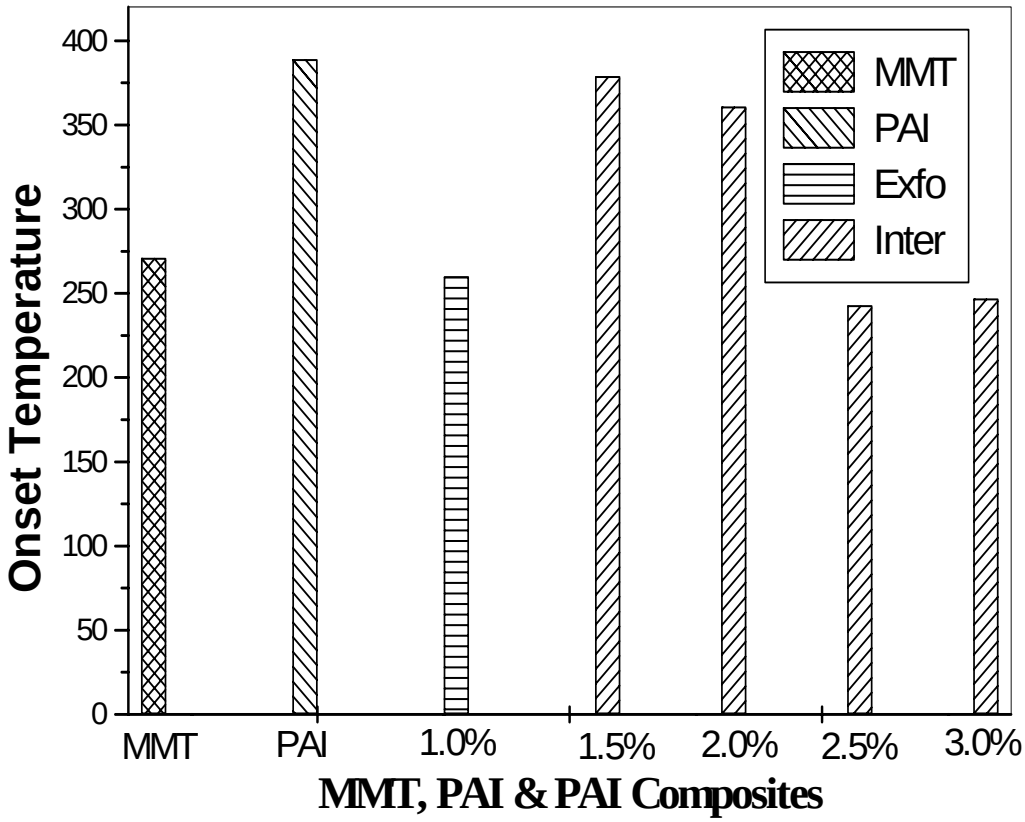

Figure 5.34 Bar chart showing onset temperatures for individual systems.

The onset temperature is a temperature at which weight loss takes place in the sample. The blank PAI shows the initial weight loss of around 10% by weight at around 275^{o}C. This initial loss of only 10% is due to a process called imidization. During imidization, water is formed and causes the scission of the polymer chains. A second weight loss for PAI was observed around 520^{o}C due to the degradation of organic matter. The high onset temperature clearly indicates the high thermal stability of PAI.

Results at various clay concentrations are however mixed. At 1.0% clay concentration (exfoliated dispersion) the onset temperature was found to be 260^{o}C.

Increase in clay concentration 1.5% and 2.0% (both showing intercalation) the onset temperature was found to be 379^{o}C and 361^{o}C respectively. Further increase in clay concentration (2.5% and 3.0%, both showing intercalation's) the onset temperature dropped to 243^{o}C and 247^{o}C respectively.

If we look carefully, the onset temperatures of MMT, 1.0%, 2.5% & 3.0% clay concentration are very close. The onset temperature of MMT is 271^{o}C, which is very low compared to PAI (389^{o}C). In case of the exfoliated dispersion (1.0%), the quaternary alkyl ammonium cations are scattered throughout the matrix without any protection. These cations are less stable towards temperature, and these are the ones who will leave the matrix first. As we recall from our diffraction data (**Figure 5.15**), a very high structural regularity (intense reflections) was observed at 1.5% and 2.0% clay concentration. In case of intercalation finite penetration of polymer chains resulted in expansion of silicate galleries resulting in an alternate arrangement of polymer chains and silicate layers. The increased thermal stability is due to hindered outdiffusion of the volatile decomposition products.

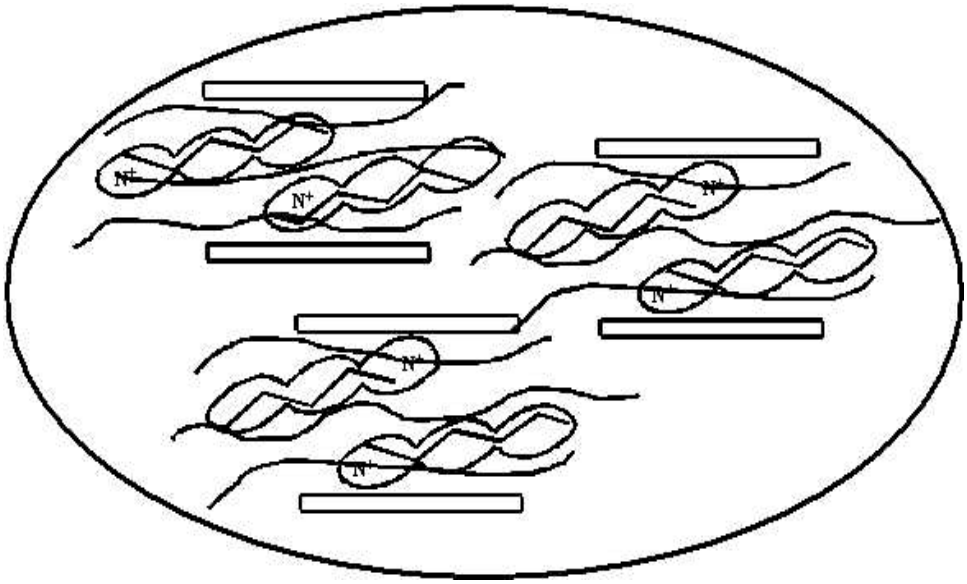

Figure 5.35 Intercalated dispersion

As seen in **Figure 5.35** the clay platelets act as a protective layers for polymer chains as well as alkyl ammonium cations. Increase in onset temperature for 1.5% and 2.0% is due to the protection effect. In the case of 2.5 and 3.0% onset temperature dropped, though intercalated dispersion was observed. Optical microscopy showed initial signs of clay agglomeration at 2.5 and 3.0% clay concentration. Diffraction results showed absence of structural regularity, which means some of the clay platelets, are not intercalated. These clay agglomerates do not show any affinity towards polymer chains and maintain their identity. The drop in onset temperature corresponds to loss of alkyl ammonium cations from these clay agglomerates.

Table 5.1 Data of onset temperature and percentage weight loss

Composition	Onset Temperature (^oC)*	Half Width (^oC)**	Weight Loss (%)***
Montmorillonite	271	323	20.45
PAI (Blnk)	389	403	9.91
1.0% Composite	260	299	11.15
1.5% Composite	379	397	8.85
2.0% Composite	361	381	10.15
2.5% Composite	243	298	18.31
3.0% Composite	247	300	16.69

* Initial weight reduction onset temperature

** Half Width at initial weight reduction onset temperature

*** Percentage weight loss at initial weight reduction

5.4.2 Conclusions Based on Degradation Studies

The thermal stability of PAI was not sacrificed due to presence of surfactant between the MMT galleries. Onset temperature was found to be dependent on the type of dispersion as well as structural regularity within the dispersion. Initial weight loss of 20% in MMT was due to degradation of alkyl ammonium cations.

5.5 Mechanical Properties

PAI + MMT nanocomposite was investigated on mechanical behavior basis. Vickers hardness test measured the hardness of PAI and PAI + MMT nanocomposites.

5.5.1 Vickers Hardness

Figure 5.36 shows the Vickers hardness of PAI and PAI + MMT nanocomposites of different MMT concentration.

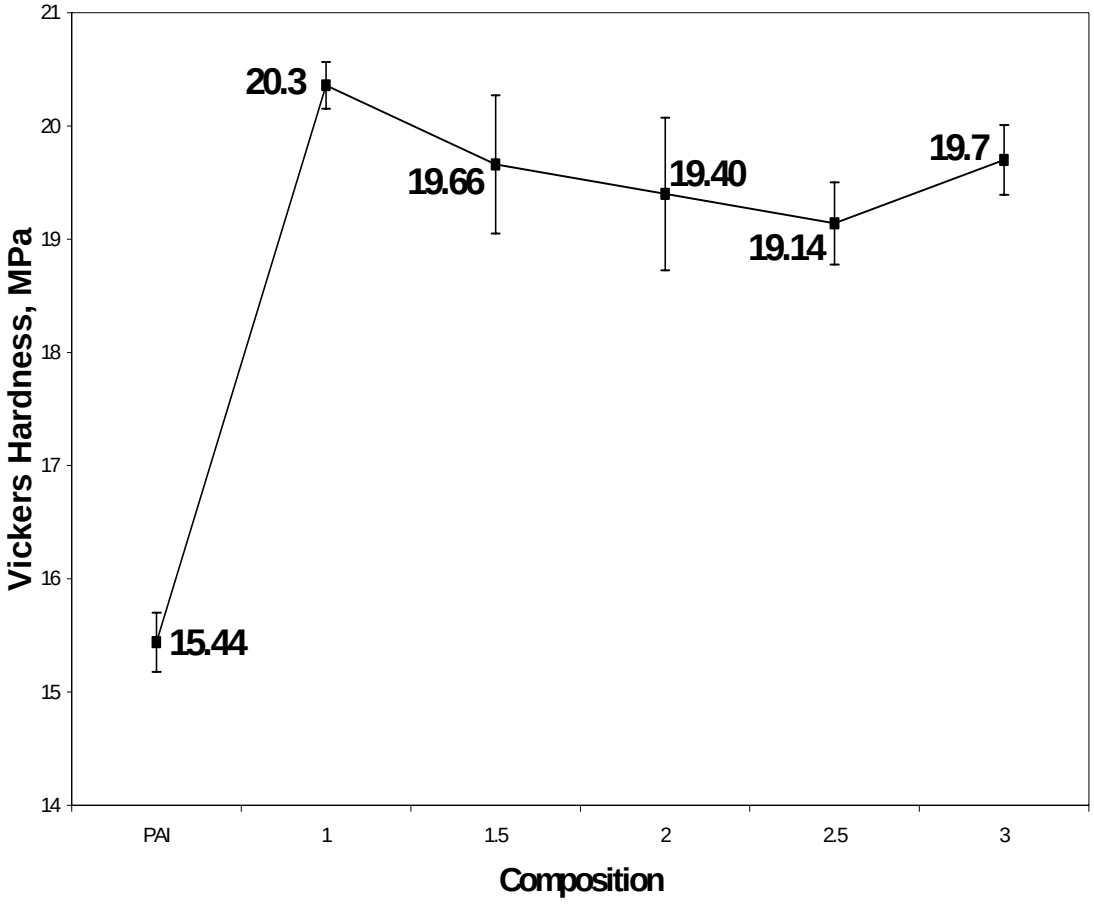

Figure 5.36 Vickers hardness of PAI and PAI + MMT nanocomposites

Addition of MMT showed marked increase in hardness of around 32%. At 1.0%, which showed exfoliated behavior, highest hardness was observed. As exfoliated dispersion clay platelets were uniformly distribute over entire matrix, this improved the stiffness of PAI. Presence of these stiff clay platelets and entanglement of polymer chains made PAI nanocomposite harder. Intercalated dispersion showed almost similar harnesses where polymer chains penetrated into silicate galleries. Finite penetration of polymer chains does not improve the hardness of PAI mainly due to retention of clay structure. The hardness however was found close to exfoliated dispersion is due to the fact that increase in concentration of MMT over exfoliated (1.0%) dispersion.

5.5.2 Conclusions Based on Hardness Behavior

Addition of MMT increased the hardness of PAI from 15 MPa to 20 MPa. Dispersion dependent mechanical properties were obtained where the exfoliated dispersion showed the highest hardness compared to intercalated dispersions.

Chapter 6

SUMMARY

A PAI + MMT nanocomposite was successfully developed. Concentration dependent dispersion behavior was observed. At low MMT concentration (1.0%) polymer/clay interactions overcame the Van der Waals interactions between silicate galleries resulting in an exfoliated dispersion with complete disruption of clay structure. This was evidenced by the absence of the peak corresponding to the basal layer spacing in XRD and TEM micrographs. Increasing the clay concentration (1.5-3.0%) resulted in an intercalated dispersion. At higher clay concentrations, Van der Waals interactions dominated over polymer clay interactions. Finite expansion in silicate galleries was observed with retention of clay structure.

The DSC study showed dispersion dependent glass transition temperature (T_g). An increase in T_g was observed for an exfoliated dispersion over the base resin. The effect of chain confinement effect affected the T_g for all intercalated dispersions. When the degree of platelet separation was small, a higher Tg was obtained. At higher platelet separations, the matrix between clay platelets had similar molecular mobility to the pure PAI matrix.

Degradation study showed PAI thermal stability was not sacrificed due to presence of surfactants (alkyl ammonium cations) between silicate galleries. When the

chains were shielded between the platelets enhanced thermal stability was obtained. The exfoliated structure resulted in the highest increase in surface hardness.

References

[1] Wang Z and Pinnavaia TJ, Chem. Mater. 1998; 10: 1820.

[2] Pinnavaia TJ, Science 1983; 220: 365.

[3] Wang MS and Pinnavaia TJ, Chem. Mater. 1994; 6: 468.

[4] Lan T, Kaviratna PD and Pinnavaia TJ, J. Phys. Chem. Solids 1996; 57: 1005.

[5] Kaviratna PD, Pinnavaia TJ and Schroeder PA, J. Phys. Chem. Solids 1996; 57:12: 1897.

[6] Bidadi H, Schroeder PA and Pinnavaia TJ, J. Phys. Chem. Solids 1998; 49:12: 1435.

[7] Lan T and Pinnavaia TJ, Chem. Mater. 1994; 6: 2216.

[8] Wang Z and Pinnavaia TJ, Chem. Mater. 1998; 10: 3769.

[9] Lan T, Kaviratna PD and Pinnavaia TJ, Chem. Mater. 1994; 6: 573.

[10] Lan T, Kaviratna PD and Pinnavaia TJ, Chem. Mater. 1995; 7: 2144.

[11] Krishnamoorti R, Vaia Ra and Giannelis EP, Chem. Mater. 1996; 8: 1728.

[12] Vaia RA, Sauer BB, Tse OK and Giannelis EP, J. Polymer Sci. 1997; 35: 59.

[13] Vaia Ra, Vasudevan S, Krawiec W, Scanlan LG and Giannelis EP, Adv. Mater. 1995; 7:2: 154.

[14] Vaia Ra, Jandt KD, Kramer EJ and Giannelis EP, Chem. Mater. 1996; 8: 2628.

[15] Vaia RA and Giannelis EP, Macromolecules 1997; 30: 8000.

[16] Vaia RA and Giannelis EP, Macromolecules 1997; 30:7990.

[17] Giannelis EP, J. Minerals 1992; 44:3: 28.

[18] Messersmith PB and Giannelis EP, Chem. Mater. 1994; 6: 1719.

[19] Messermith PB and Giannelis EP, J. Polymer Sci. 1995; 33: 1047.

[20] Burnside SD, Wang HC and Giannelis EP, Chem. Mater. 1999; 11: 1055.

[21] Giannelis EP, Chem. Mater. 1990; 2: 627.

[22] Messersmith PB and Giannelis EP, Chem. Mater. 1993; 5: 1064.

[23] Messersmith PB and Giannelis EP, J. Polymer Sci. 1995; 33: 1047.

[24] Krishnamoorti R and Giannelis EP, Macromolecules; 30: 4097.

[25] Giannelis EP, Adv. Mater. 1996; 8:1: 29.

[26] Burnside SD and Giannelis EP, Chem. Mater. 1995; 7:9: 1597.

[27] McKenna GB, Conference Proceedings ANTEC, 2000; Vol. II: 2004.

[28] Chang JH, Park DK, Ihm KJ, J. Polymer Sci. 2001; 39: 471.

[29] Kojima Y, Fukumori K, Usuki A, Okada A and Kurauchi T, J. Mater. Sci. Letters 1993; 12: 889.

[30] Kojima Y, Usuki A, Kawasumi M, Okada A, Fukushima Y, Kurauchi T and Kamigaito O, J. Mater. Res. 1993; 8:5: 1185.

[31] Weiss A, Chem. International Edit. 1963; 2: 134.

[32] Kurokawa Y, Yasuda H, Kashiwagi M and Oyo A, J. Mater. Sci. Letters 1997; 16: 1670.

[33] Yano K, Usuki A, Okada A, Kurauchi T and Kamigaito O, J. Polymer Sci. 1993; 31: 2493.

[34] Usuki A, Kojima Y, Kawasumi M, Okada A, Fukushima Y, Kurauchi T and Kamigaito O, J. Mater. Res. 1993; 8:5: 1179.

[35] Usuki A, Kojima Y, Kawasumi M, Okada A, Fukushima Y, Kurauchi T and Kamigaito O, J. Mater. Res. 1993; 8:5: 1174.

[36] Moet AS and Akclah A, Mater. Letters 1993; 18: 97.

[37] Gardolinski JE, Carrera LCM, Cantao MP, Wypych F, J. Mater. Sci 2000; 35: 3113.

[38] Limary R, Swinnea S and Green PF, Macromolecules 2000; 33: 5227.

[39] Ozin GA, Advanced Materials 1992; 4:10: 612.

[40] Best AS, Ferry A, MacFarlane DR and Forsyth M, Solid State Ionics 1999; 126: 269.

[41] Hackett E, Manias E and Giannelis EP, J. Chemical Phys. 1998; 108:17: 7410.

[42] Jimenez C, Ogata N, Kawai H and Ogihara T, J. Applied Polymer Sci. 1997; 64: 2211.

[43] Kojima Y, Usuki A, Kawasumi M, Okada A, Kurauchi T and Kamigaito O, J. Polymer Sci. 1993; 31: 983.

[44] Shia D, Hui CY, Burnside SD and Giannelis EP, Polymer Composites 1998; 19:5: 608.

[45] Kojima Y, Usuki A, Kawasumi M, Okada A, Kurauchi O, Kamigaito O and Kaji K, J. Polymer Sci 1994; 32: 625.

[46] Kojima Y, Matsuoka T, Iakahashi H and Kurauchi T, J. Applied Polymer Sci. 1994; 51: 683.

[47] Ratto JA, Steeves DM, Powell BE, Conference Proceedings ANTEC 1999; Vol II: 1628.

[48] Kurokawa Y, Yasuda H, Kashiwagi M and Oyo A, J. Mater. Sci. Letters 1997; 16: 1670.

[49] Kelly P, Akelah A, Qutubuddin S and Moet A, J Mater. Sci. 1994; 29:9: 2274.

[50] Akkspeddi MK, Conference Proceedings ANTEC 1999; Vol II: 1619.

[51] Chen TK, Tien YI and Wei KH, J. Polymer Sci. 1999; 37: 2225.

[52] Polymer Melt Intercalation in Mica-Type Layered Silicates, Vaia RA, Ph.D. Thesis May 1995; Cornell University, USA.

[53] Nanocomposites of Polymers and Layered Silicates, Shen Z, Ph.D. Thesis Oct 2000; Monash University, Australia.

[54] Synthesis and Characterization of Thermoset-Clay Nanocomposites, Kornmann X, Report, Lulea University of Technology, Sweden.

[55] Dagani R, Chemical & Engineering News, 1999; 77:23: 25.

[56] Miller B, Plastics Formulating & Compounding, May/June 1997; 30.

[57] Sherman LM, Plastics Technology, June 1999; 52.

[58] Fitzpatrick J., Engineered Materials Handbook Vol. 2, ASM International, 1995; 128-137.

[59] Olphen HV, An Introduction to Clay Colloid Chemistry, John Wiley & Sons1977; 57-76.

[60] Brundle R. C., Evans C., Wilson S., Encyclopedia of Materials Characterization, Butterworth-Heinemann, 1992; 60-69.

[61] Brundle R. C., Evans C., Wilson S., Encyclopedia of Materials Characterization, Butterworth-Heinemann, 1992; 198-213.

[62] Willard D., Dean J., Instrumental Methods of Analysis, D. Van Nostrand Company, 1974; 258-301.

[63] Brundle R. C., Evans C., Wilson S., Encyclopedia of Materials Characterization, Butterworth-Heinemann, 1992; 99-114.

[64] Brundle R. C., Evans C., Wilson S., Encyclopedia of Materials Characterization, Butterworth-Heinemann, 1992; 70-83.

[65] Dodd J., Tonge K., Thermal Methods, John Wiley & Sons, 1987; 110-139.

[66] Dodd J., Tonge K., Thermal Methods, John Wiley & Sons, 1987; 40-96.

[67] Dieter G. E., Mechanical Metallurgy, McGraw-Hill Book Company, 1988; 325-332.